NASA TECHNICAL NOTE

NASA TN D-7899

NASA TN D-7899

(NASA-TN-D-7899) FLIGHT PERFORMANCE OF A NAVIGATION, GUIDANCE, AND CONTROL SYSTEM CONCEPT FOR AUTOMATIC APPROACH AND LANDING OF SPACE SHUTTLE ORBITER (NASA) 68 p HC $4.25 CSCL 22B H1/18

N75-16612

Unclas 10081

FLIGHT PERFORMANCE OF A NAVIGATION, GUIDANCE, AND CONTROL SYSTEM CONCEPT FOR AUTOMATIC APPROACH AND LANDING OF THE SPACE SHUTTLE ORBITER

Frederick G. Edwards, John D. Foster, Daniel M. Hegarty, Donald W. Smith, Fred J. Drinkwater III, and Rodney C. Wingrove

Ames Research Center
Moffett Field, Calif. 94035

FEB 1975 RECEIVED

NATIONAL AERONAUTICS AND SPACE ADMINISTRATION • WASHINGTON, D. C. • FEBRUARY 1975

1. Report No.	2. Government Accession No.	3. Recipient's Catalog No.
NASA TN D-7899		

4. Title and Subtitle	5. Report Date
FLIGHT PERFORMANCE OF A NAVIGATION, GUIDANCE, AND CONTROL SYSTEM CONCEPT FOR AUTOMATIC APPROACH AND LANDING OF THE SPACE SHUTTLE ORBITER	February 1975
	6. Performing Organization Code

7. Author(s)	8. Performing Organization Report No.
Frederick G. Edwards, John D. Foster, Daniel M. Hegarty, Donald W. Smith, Fred J. Drinkwater III, and Rodney C. Wingrove	A-5321
	10. Work Unit No. 502-33-81

9. Performing Organization Name and Address	11. Contract or Grant No.
NASA Ames Research Center Moffett Field, Calif. 94035	
	13. Type of Report and Period Covered
12. Sponsoring Agency Name and Address	Technical Note
National Aeronautics and Space Administration Washington, D. C. 20546	14. Sponsoring Agency Code

15. Supplementary Notes

16. Abstract

Unpowered automatic approaches and landings were conducted to study navigation, guidance, and control problems associated with terminal area approach and landing for the Space Shuttle vehicle.

The flight tests were performed in a Convair 990 aircraft equipped with a digital flight control computer connected to the aircraft control system and displays. The tests were designed to evaluate the performance of a navigation and guidance concept that utilized blended radio/inertial navigation with VOR, DME, and ILS as the ground navigation aids. The results from 36 automatic approaches and landings from 11,300 m (37,000 ft) to touchdown are presented. Preliminary results indicate that this concept may provide sufficient accuracy to accomplish automatic landing of the shuttle orbiter without air-breathing engines.

17. Key Words (Suggested by Author(s))	18. Distribution Statement
Autoland Space shuttle landing Terminal area guidance	Unclassified – Unlimited STAR Category–18

19. Security Classif. (of this report)	20. Security Classif. (of this page)	21. No. of Pages	22. Price*
Unclassified	Unclassified	68	$4.25

*For sale by the National Technical Information Service, Springfield, Virginia 22151

TABLE OF CONTENTS

PRECEDING PAGE BLANK NOT FILMED

SYMBOLS

ADDAS	airborne digital data acquisition system
A_i, i = 1, 2, . . . 5	integrator gains
ARC	Ames Research Center
CADS	central air data system
CAS	calibrated airspeed
C_i, i = 1, 2, . . . 8	constants
$\mathbb{C}_L$	centerline
DME	distance measuring equipment
EAFB	Edwards Air Force Base (USAF)
FRC	Flight Research Center
g	gravitational constant
GSIP	glide-slope intercept point
G/S	ILS glide slope
H, h	altitude (H = −Z)
IAS	indicated airspeed
ILS	instrument landing system
INS	inertial navigation system
K_i, i = 1, 2, . . . 17	gains
L/D	aerodynamic lift-to-drag ratio
LOC	ILS localizer
Q	dynamic pressure
R	distance to center of specified circle
RCS	runway coordinate system
R_0	R-zero circle
s	Laplace operator
SB	speed brakes
SS-FTS	simulated shuttle flight test system
SSV	Space Shuttle vehicle
TACAN	tactical air navigation
TCG	time code generator
TOL	takeoff and landing facility
UFH	ultra high frequency
V	velocity
VHF	very high frequency
VOR	very high frequency omnirange
WWV	radio call letters of the National Bureau of Standard time transmission
X, Y, Z	longitudinal, lateral and vertical coordinate in RCS
α	angle of attack
γ	flight path angle
ϵ	error
θ	pitch attitude

σ	standard deviation
τ	time constant
ϕ	roll attitude
ψ	heading angle
$(\dot{})$	time derivative
$(\ddot{})$	time double derivative
$(\hat{})$	estimate
$(\bar{})$	measured

Subscripts

Baro	barometric
c	command
cf	center of final turn circle
cr	center of R-zero circle
err	error
ew	east-west
Gnd	ground
i	inertial
INS	inertial navigation system
ns	north-south
o	final flare engage
p	predictive or feedforward command
ref	reference
R	radar (ground based measurement)
RAD	radar (onboard radar altimeter measurement)
syn	synchronization
tan	tangent to R-zero circle
T	true

FLIGHT PERFORMANCE OF A NAVIGATION, GUIDANCE, AND CONTROL SYSTEM CONCEPT FOR AUTOMATIC APPROACH AND LANDING OF THE SPACE SHUTTLE ORBITER

Frederick G. Edwards, John D. Foster, Daniel M. Hegarty, Donald W. Smith,
Fred J. Drinkwater III, and Rodney C. Wingrove

Ames Research Center

SUMMARY

Unpowered automatic approaches and landings were conducted to study navigation, guidance, and control problems associated with terminal area approach and landing for the Space Shuttle vehicle.

The flight tests were performed in a Convair 990 aircraft equipped with a digital flight control computer connected to the aircraft control system and displays. The tests were designed to evaluate the performance of a navigation and guidance concept that utilized blended radio/inertial navigation with VOR, DME, and ILS as the ground navigation aids. The results from 36 automatic approaches and landings from 11,300 m (37,000 ft) to touchdown are presented. Preliminary results indicate that this concept may provide sufficient accuracy to accomplish automatic landing of the shuttle orbiter without air-breathing engines.

INTRODUCTION

The concept of the Space Shuttle vehicle includes the recovery of the Shuttle Orbiter by automatic or manual landing on a conventional size runway in instrument weather conditions. The similarities with the landing of a current-day jet transport are apparent, but there are differences that prevent a direct transfer of current autoland technology. For example, the Space Shuttle will have a lower maximum lift/drag ratio and may be unpowered during the approach and landing. Consequently, it may not have a go-around capability, and the terminal area guidance technique must effectively manage the available energy.

As a basis for defining design requirements for the terminal phase of the shuttle mission, a program was initiated at ARC to develop a guidance, navigation, and control concept, and to demonstrate its performance in an inflight simulation of shuttle approach and landing maneuvers. At the time this study was initiated, the orbiter design had a maximum subsonic lift/drag ratio of 6.7, which established the geometry for the landing profiles used. Program guidelines included:

1. Are air-breathing engines needed to assist in terminal area approach and landing?

2. What are suitable airborne and ground-based elements for the shuttle navigation system?

3. What are the acceptable shuttle velocities and rate of descent for approach and landing?

4. What are runway size requirements?

5. Are there problems associated with the selection of a digital flight system?

The flight investigations of references 1 and 2 have demonstrated the effectiveness of using elementary guidance and navigation aids in landing low lift/drag ratio unpowered aircraft. All these approaches were flown under manual control and in good visibility conditions. In the development of the automatic landing concepts, comprehensive analysis and ground-based simulation studies were performed (refs. 3–9). These background studies included the definition and analysis of several approach and landing system concepts (refs. 3 and 5); a study of the automatic flare and decrab maneuver (ref. 6); studies of navigation accuracies using blended radio and inertial navigation information (refs. 7 and 8); a study of the handling-qualities criteria for the shuttle during the terminal phase of flight (ref. 9); and the final system design and candidate aircraft selection studies for the flight test (ref. 4), which resulted in the choices of the Ames Convair 990 aircraft as the test vehicle.

As a result of these studies the NASA contracted with Sperry Flight Systems Division to provide a suitable avionics system of sufficient size, speed, and flexibility to mechanize the guidance, navigation, and control concepts postulated for the landing of the shuttle orbiter. A programmable digital computer system was chosen for this purpose.

Installation and checkout of the system in the CV-990 aircraft was completed in June 1972, and flight tests were initiated soon after. A total of 18 flights have been conducted during three flight test periods in June, August, and October-November 1972.

The initial stages of these tests consisted of functional checkout and formal acceptance of the system. The latter portion of the tests, primarily the October-November test series, was devoted to recording system performance data, including touchdown statistics for a single autoland concept. Preliminary results of the tests were presented in references 10, 11, and 12. This report includes (1) a description of the functional mechanization of the guidance, navigation, and control concept; (2) discussion of the avionics system operation, and the test operations at Edwards AFB; and (3) the results of the final data analysis.

The versatile digital avionics system installed in the CV-990 aircraft provides a unique facility with considerable flexibility and a potential capability for the study of a broad spectrum of terminal area problems presented by Space Shuttle, as well as research on noise abatement and energy-management approach techniques for conventional jet transports. The CV-990 system also represents successful implementation of a digital flight control system for CTOL aircraft. The concept development and fabrication of this system, and the operational procedures developed in simulation and verified in flight, have yielded a valuable data base of information. This information can be used by designers and operators of advanced CTOL aircraft avionics systems in configuring the system and developing operational procedures for terminal area operations.

GUIDANCE, NAVIGATION, AND CONTROL SYSTEM OPERATION

A general discussion of the operation of the guidance, navigation, and control system is presented in this section. Further detailed information is provided in reference 12, which presents and discusses the complete set of guidance, navigation, and control equations.

System Concepts

Landing a large unpowered vehicle with low L/D requires a strategy for energy management. The speed and altitude profile is configured to maintain a level of energy in excess of that required to reach the touchdown point. The strategy consists of dissipating this excess energy in a controlled fashion so that the proper landing conditions are established. The vehicle energy can be controlled through shaping of the trajectory (e.g., path stretching) and through proportional deployment of speed brakes. In the system concept demonstrated in the subject tests, the trajectory is shaped to vary the path length over which the vehicle flies for energy modulation during the high-altitude portion of the approach. During the final approach, the vehicle flies a two-segment fixed flight path, utilizing speed brakes for vehicle energy control. The speed brakes are effective in controlling speed on the approach and in minimizing touchdown dispersions resulting from head and tail winds. The technique of landing unpowered vehicles by use of a high-energy, steep glide-path approach followed by a flare to a shallow decelerating final approach dates back many years and is a recommended landing procedure for engine-out conditions on many aircraft. Thus, enegy management through path stretching and two-segment approach paths used herein does not involve new aerospace concepts.

The pilot's role during the flight investigation of the automatic landing system was that of a system performance monitor, viewing the progress of the flight using the outside visual scene and the cockpit displays. Although the avionics system has provisions for manual backup modes, these were not fully evaluated and are not reported herein.

Guidance Functions

The guidance system has two main functions. One is to compute a reference flight path that will take the aircraft from a range of initial locations and guide it to a safe landing on the runway at the desired touchdown position and velocity. The other is to provide the pitch- and roll-attitude commands necessary to follow the reference path without exceeding aircraft operational limitations.

The reference flight path used in this system is only one of several possibilities for the unpowered Space Shuttle vehicle terminal area energy management. However, most energy management methods use flight path elements such as a target circle, an outbound segment for path stretching, and a steep glide path, which are similar to those used in this system. The details of the SS-FTS reference flight path are shown in figure 1.

In the lateral plane, the reference flight path begins at the current aircraft position (point A, fig. 1), and follows a straight line tangent to the R-zero (target) circle at point B (fly to R_0 mode). The aircraft flies along the tangent line onto the circle and follows the circle to point C (track R_0 mode), where it intercepts the "outbound radial," a straight line tangent to the circle and at an angle of 20° to the runway centerline. It then follows the radial (radial track mode) to point D, whose location on the radial is a variable computed by the guidance equations. At point D, the aircraft follows the "final turn" circle (final turn mode), which is tangent to both the radial and the runway centerline. After this final turn segment, the aircraft follows the runway centerline extension (track runway mode) to the runway.

In the vertical plane, the aircraft does not initially follow a computed path as it does in the horizontal plane. Instead, it flies a specified lift/drag ratio (operational L/D mode), which results in a glide angle of about 7°. However, after completing the final turn segment in the horizontal plane, the aircraft intercepts the computed 10° "steep glide slope" at point F, which it follows (steep G/S track mode) until it reaches a point 427 m (1400 ft) above the ground. It then flares (first flare mode) onto the 2.5° ILS glide slope, which it follows (shallow G/S track mode) down to an altitude of 18 m (60 ft) where it flares (final flare mode) onto the runway and touches down.

For descriptive purposes, the guidance modes that command the aircraft to follow the reference trajectory can be divided into two categories: high-altitude energy management guidance and low-altitude guidance. The high-altitude section comprises the modes used before the aircraft intersects the steep glide slope, normally above 6,100 m (20,000 ft), and the low altitude section comprises those used after steep glide-slope capture.

The high-altitude lateral modes begin with the fly to R mode. The roll-angle command is given by

$$\phi_C = K_1(\psi_{tan} - \psi)$$

where ψ is the aircraft heading with respect to the runway, ψ_{tan} is the bearing of the line, tangent to the R-zero circle and passing through the estimated aircraft position, and K_1 is the gain. When the aircraft flies to within 732 m (2400 ft) of the circle perimeter, the guidance switches to the track R-zero circle mode. Then the roll-angle command is given by

$$\phi_C = \tan^{-1}\frac{V_i^2}{gC_1} + K_2\,(R_{cr} - C_1 + K_3\dot{R}_{cr})$$

where V_i is the inertial velocity, C_1 is the radius of the circle, g is the gravitational acceleration constant, R_{cr} is the distance from the aircraft to the center of the circle, $\dot{R}_{cr}$ is the time derivative of R_{cr}, and K_2 and K_3 are gains. As the aircraft tracks the circle, the guidance system compares aircraft heading to the outbound radial bearing. When the heading is within 15° of the radial bearing, the guidance switches to the radial track mode. If the aircraft approaches from the left of the radial, the guidance switches to radial track when the aircraft heading is within 45° of the radial bearing. The roll-angle command in this mode is given by

$$\phi_C = K_4\left[(\hat{X} - C_7)\sin 20° + \hat{Y}\cos 20° + K_5\left(\hat{\dot{X}}\sin 20° + \hat{\dot{Y}}\cos 20°\right)\right]$$

where $\hat{X}$ and $\hat{Y}$ are the coordinates of the estimated aircraft position, $\dot{\hat{X}}$ and $\dot{\hat{Y}}$ are the estimated aircraft inertial velocity components, C_7 is the location of the outbound radial interception of the runway centerline extension, and K_4 and K_5 are gains. By varying the length of the radial path, the aircraft energy is adjusted so that it can capture the steep glide slope at or above an altitude of 6,100 m (20,000 ft). The system continuously computes the location of the center and the magnitude of the radius of the final turn circle that intercepts the radial at the aircraft's estimated position and is tangent to the runway centerline extension. These coordinates and the estimated flight path angle are used to computer two altitude terms h_1 and h_2. The term h_1 is the altitude that the aircraft would lose during the final turn maneuver, and h_2 is the height of the steep glide slope at a point where the final turn circle meets the runway centerline extension. Hence, the sum of h_1 and h_2 is the desired aircraft altitude at the beginning of the final turn if the aircraft is to acquire the steep glide slope at the end of the final turn. When the sum of h_1 and h_2 equals the aircraft altitude, the guidance system switches to the final turn mode. Then the roll-angle command is given by

$$\phi_c = \tan^{-1} \frac{V_i^2}{gY_{cf}} + K_6 (R_{cf} - Y_{cf} + K_7 \dot{R}_{cf})$$

where Y_{cf} is the computed radius of the final turn circle, R_{cf} is the distance from the aircraft to the center of the final turn circle, and K_6 and K_7 are gains. When the aircraft heading is within 30° of the runway bearing, the guidance switches to the track runway centerline mode in which the roll commands are given by

$$\phi_c = K_8 \left[\hat{Y} \left(1 + \frac{A_1}{s} \right) + K_5 \dot{\hat{Y}} \right]$$

where $\hat{Y}$ is the estimated aircraft displacement off the runway centerline extension, K_8 and K_5 are gains, A_1 is the integral gain, and s is the Laplace operator.

While each of the preceding modes are in effect, the pitch guidance is in the operational L/D mode. The pitch guidance controls the aircraft to fly near the L/D that maximizes the glide range. Here the pitch-attitude command is given by

$$\theta_c = K_9 (Q - Q_{ref})$$

where

$$Q_{ref} = C_2 + \frac{A_2}{s} (\hat{\alpha} - \alpha_{ref})$$

and Q is the dynamic pressure, $\hat{\alpha}$ is the estimated angle of attack, C_2 is a constant, K_9 and A_2 are gains, and α_{ref} is the angle-of-attack reference, which is a function of vehicle weight and Mach number. This reference is about 2° less than the angle of attack for maximum L/D. It does not equal the maximum L/D angle since some control margin is needed to keep the aircraft on the "front side" of the L/D-versus-airspeed curve. While the guidance is in this mode, the aircraft calibrated airspeed averages about 230 knots.

When the aircraft intercepts the steep glide slope, usually at an altitude of about 6,100 m (20,000 ft), the guidance system begins using the low-altitude modes. The lateral guidance remains in the runway centerline tracking mode, but the pitch guidance switches to the steep glide-slope tracking mode. The pitch-attitude command is then given by

$$\theta_c = K_{10}\left(\gamma_{ref_1} - \hat{\gamma}\right) + K_{11}H_{err}\left(1 + \frac{A_3}{s}\right)$$

where

$$H_{err} = (\hat{X} - C_8)\tan\gamma_{ref_1} - \hat{h}$$

and γ_{ref_1} is the steep glide-slope angle ($-10°$), $\hat{\gamma}$ is the estimated aircraft glide angle, $\hat{X}$ is the x coordinate of estimated aircraft position, C_8 is the steep glide-slope ground intercept point, $\hat{h}$ is the estimated aircraft altitude above ground level, K_{10} and K_{11} are gains, and A_3 is an integral gain.

As the aircraft descends along the steep glide slope, the airspeed increases to an equilibrium value determined by the aircraft L/D and the winds. When no winds are present, a nominal value of 305 knots indicated airspeed is achieved. To compensate for any airspeed vairations caused by winds, the guidance system commands a speed brake setting when the aircraft is 762 m (2500 ft) above the ground. The speed-brake command is given by

$$\text{Speed brake} = \text{INT}\left[\frac{350V_i + (1/2)W - 92{,}500}{5000} - 29.5\right] \cdot 5°$$

where INT[ ] is a function that takes the integer value of the enclosed quantity and W is the aircraft weight. This command is resolved into 5° increments since the speed brakes cannot be positioned with any greater accuracy.

Shortly after the pilot sets the speed brakes, according to the command, the aircraft descends to a point on the steep glide slope that is 0.97° above the center of the ILS glide-slope beam; altitude is ≅427 m (1400 ft). At this point, the pitch guidance switches to the first flare mode in which the pitch-attitude command is given by

$$\theta_c = K_{12}\left(\theta_{c_6} + \gamma_{syn} - \hat{\gamma}\right) + \theta_{c_6} + \frac{1}{Q}\left(C_3 - \frac{\dot{V}_T}{V_T}\,\frac{C_4}{s}\right)$$

where

$$\theta_{c_6} = \int_{t_c}^{t_x} \frac{V_i}{360}\,dt$$

t is the time when $\theta_{c_6} = \gamma_{ref_2} - \gamma_{syn}$, γ_{syn} is $\hat{\gamma}$ at phase engage, V_T is true airspeed, $\dot{V}_T$ is the aircraft deceleration rate, γ_{ref_2} is the ILS glide-slope angle ($-2.5°$), K_{12} is a gain, and C_3 and C_4 are constants. This pitch command produces a 0.25 "g" flare onto the shallow glide slope. The shallow glide-slope tracking mode is engaged if the aircraft is either above the ILS beam and climbing away from it or below the beam and falling below it. The pitch command is given bv

$$\theta_c = \theta_{c_6} - \frac{1}{Q}\left(C_3 + \frac{C_4}{s}\,\frac{\dot{V}_T}{V_T}\right) - \frac{K_{13}}{V_T}\left(H - \hat{X}\tan\gamma_{ref_1}\right)\left(1 + \frac{A_4}{s}\right) + K_{14}\left(\gamma_{ref_2} - \hat{\gamma}\right)$$

where the terms θ_{c_6}, C_3, and C_4 are the same as in the previous mode, $\hat{X}$ is the x coordinate of the estimated aircraft position, and K_{13}, K_{14}, and A_4 are gains. As the aircraft descends below an

altitude of 137 m (450 ft), the pitch guidance begins to compute the final flare initiation altitude as a function of altitude rate derived from the radar altimeter. When the radar altitude equals 9.2 m (30 ft) plus twice the altitude rate ($H = 9.2 + 2\dot{H}$), the final flare mode is engaged. The pitch command during the flare is

$$\theta_c = \theta_p + \left[K_{15}(\dot{H}_{ref} - \hat{\dot{H}}) - K_{16}\ddot{H}\right]\left(1 + \frac{A_5}{s}\right)$$

where

$$\theta_p = \left[C_5 + K_{17}(V_{ref} - V_{T_o})\right]\left(\frac{1}{\tau s + 1}\right) + \frac{C_6}{V_T s}$$

$$\hat{\dot{H}}_{ref} = \dot{H}_o - \left[(\dot{H}_o + 3)\frac{1}{\tau s + 1}\right]$$

$\hat{\dot{H}}$ is the altitude rate derived from the radar altimeter signal, $\ddot{H}$ is the aircraft vertical acceleration, V_{ref} is the nominal true airspeed at final flare engage, V_{T_o} is the actual true airspeed at final flare engage, $\dot{H}_o$ is the altitude rate at phase engage, τ is the flare time constant, C_5 and C_6 are constants, and K_{15}, K_{16}, A_5 and K_{17} are gains. With no wind disturbances, these commands cause the aircraft to acquire a vertical descent rate of 0.6 m/sec (2 ft/sec) at about 2.5 m (8 ft) above the ground and to hold that at rate until touchdown. When the 2.5-m altitude is reached, the lateral guidance switches to the decrab mode, which computes a rudder command proportional to the error between aircraft heading and runway heading (crab angle). This command aligns the aircraft with the runway causing a side-slip angle to develop. To offset the resulting roll moment, the decrab mode also computes an aileron command proportional to the original crab angle.

In all the guidance modes, limits are imposed on the commands to keep all maneuvers within the capability of the aircraft. All pitch commands are rate limited so that the vertical accelerations do not exceed 0.8 g. The roll commands are limited to a rate of 15°/sec and are limited in magnitude according to aircraft altitude. Above 4,570 m (15,000 ft), the roll limit is 45°; below 4,570 m and above 1,520 m (5,000 ft), the limit is 30°; and below 1,520 m, the limit is 15°.

Energy management window— As with any guidance concept, there are certain performance limitations. Specifically, the high-altitude guidance modes are limited in energy control by the aircraft L/D. This limit is shown in figure 2 as an energy window at 11,300 m (37,000 ft) above the ground. The energy window, or maximum range boundary indicated by the cardioid, is the area from which the aircraft can initiate an approach, capture the runway centerline and steep glide slope at an altitude above 6,100 m (20,000 ft), and reach the runway with a safe landing velocity. The size and shape of the energy window was established with the following conditions: (1) the vehicle heading at 11,300 m (37,000 ft) altitude is aimed at the point of tangency on the R-zero circle; (2) the vehicle flies a constant L/D glide path until capture of the steep glide slope; (3) there are no winds. If any of these conditions is violated, the window obviously is changed.

Although not considered a significant constraint, the initial vehicle velocity at 11,300 m also affects the window size. For the window presented in figure 2, the initial true airspeed is 480 knots ($M = 0.83$). A lower initial velocity will reduce the maximum range boundary; however, the effect is slight.

The shape of the boundary is primarily the result of the aircraft L/D limit, but the straight-line section to the left of the outbound radial is the result of a 45° bank-angle limit imposed on the guidance roll commands. If, for example, the aircraft approached the target circle from a position outside this section of the boundary, it could not make the left turn required to capture the radial line before the guidance switched to the final turn mode. Such a case would result in the aircraft badly overshooting the negative X axis at the end of the final turn.

Wind effects– Since headwinds reduce the glide range and tail winds increase the glide range of the aircraft, the size and shape of the energy window (fig. 2) depend on the direction and magnitude of the winds. For example, the boundary will move toward the target circle for those trajectories that face a headwind during most of the descent to 6,100 m (20,000 ft) altitude.

Winds also affect the ability of the guidance system to follow the reference trajectory during final turn mode. For example, in a minimum energy case, the lateral guidance does not follow the radial; instead, it switches from the target circle tracking to the final turn mode directly. With no winds, the resulting final turn circle requires a 45° bank angle, which is the maximum allowable. Hence, if there is a wind component in the direction of the Y axis, the aircraft will be blown off the final turn circle and will overshoot the negative X axis before acquiring it. Fortunately, the overshoots produced do not cause significant energy losses.

Simulation runs have shown that wind shears encountered after the final speed brake adjustment (below 760 m (2500 ft)) can have a significant effect on the aircraft airspeed dispersions. These dispersions could be effectively controlled if continuous modulation of the speed brake were provided.

Navigation Functions

To compute and follow the reference trajectory, aircraft position and velocity must be known. Although measurements of these quantities are available on the aircraft, nearly all measurements contain errors that would degrade the total system performance. To improve performance, the navigation system combines various measurements in complementary filters that provide a relatively error-free aircraft position estimate.

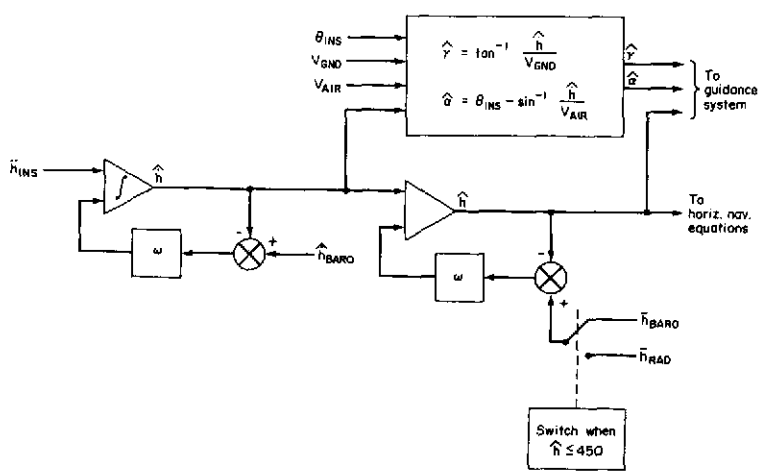

Sketch (a)

In the vertical plane, the navigation system estimates the aircraft altitude, altitude rate, flight path angle, and angle of attack from the barometric altitude, barometric altitude rate, INS vertical acceleration, and radar altitude in the complementary filter shown in sketch (a). The filter uses the altitude and altitude rate measurements to reduce the effects of the bias inherent in the inertially measured vertical acceleration. This process

provides altitude rate and altitude estimate that do not have the time lags introduced by conventional noise filters.

Since the barometric altimeter can have bias errors that are hazardous at low altitudes, the radar altimeter is used for the altitude measurement below altitudes of 137 m (450 ft). The altitude rate estimate, which is not affected by the altitude measurement, combined with true airspeed from the air data computer and pitch attitude from the INS, provides the angle-of-attack estimate. The altitude rate estimate, combined with the ground speed from the INS, provides the flight-path angle estimate. The navigation system provides another altitude rate estimate. The estimate is derived from the radar altimeter measurement as shown in sketch (b); this estimate is used only for the final flare initiation and control. This altitude rate estimate is a lagged derivative of the input and is computed continuously when the aircraft is below an altitude of 137 m (450 ft).

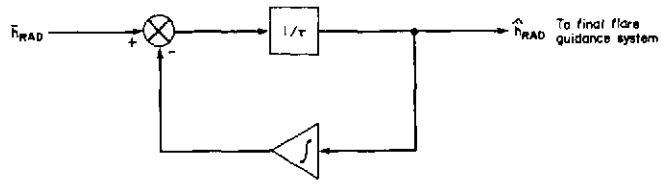

Sketch (b)

In the horizontal plane, the navigation system uses position measurements from radio navigation aids and velocity estimates from the INS to estimate the aircraft position. Three sets of radio navigation aids are used in three modes for specific segments of the trajectory. For the segment between points A and E in figure 3, where the aircraft is either above 6,100 m (20,000 ft) altitude or greater than 20 n.mi. downrange of the touchdown point, the system is in the "DME-DME NAV" mode. In this mode, the system derives the position measurement in runway coordinates using the DME range from the George TACAN, the DME range and VOR bearing from the Lake Hughes VORTAC, and the altitude estimate from the vertical navigation equations. Each DME range and the altitude estimate provide the ground plane distance from the aircraft to the DME station. Since the two ground distances give two possible solutions for the measured aircraft location in the ground plane, the VOR bearing is required to eliminate the incorrect solution.

On the trajectory segment between points E and G in figure 3, where the aircraft altitude is between 6100 m and 427 m (1400 ft) or its position is less than 20 n.mi. downrange of the touchdown point, the system is in the "DME-LOC NAV" mode. In this mode, the system derives the position measurement in runway coordinates from the Lake Hughes VORTAC DME range, the Edwards AFB ILS localizer derivation, and the altitude estimate. The DME range and the altitude estimates provide the ground plane distance from the aircraft to the DME station. This distance, combined with the DME station location and the localizer deviation, gives the location of the aircraft in the runway coordinate system.

On the trajectory segment beginning with aircraft descent to within 0.97° above the ILS glide-slope beam center (point G, fig. 3), the navigation system is in the "GS-LOC NAV" mode. Here the system derives the position measurement from the Edwards AFB glide-slope and localizer deviations, and the altitude estimate. In this case, the altitude and the glide-slope deviation yield the groundplane distance between the glide-slope transmitter and the aircraft. This distance, combined with the localizer transmitter location and the localizer deflection, gives the measured location of the aircraft in the runway coordinates. During the final flare maneuver, the navigation system remains in the GS-LOC NAV mode until the autopilot is disconnected after touchdown, although the glide-slope information is no longer used by the guidance system after final flare initiation.

The position measurements ($\bar{X}_{measurement}$, $\bar{Y}_{measurement}$) for each navigation mode are combined with the INS velocity components (V_{ns}, V_{ew}) in a complementary filter to give the position estimate as shown in sketch (c). This type of filter mechanization basically uses the position measurement to reduce the low-frequency errors in the estimate, which are caused by bias or drift errors in the INS. The filter gains are functions of each navigation mode, but they are held constant while a particular mode is in effect.

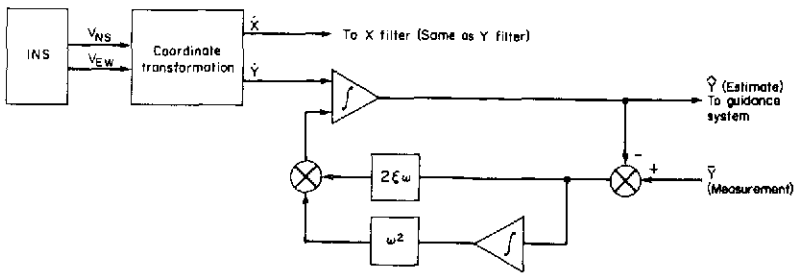

Sketch (c)

If a radio navigation aid should fail, depriving the system of position measurements, the filter continues to provide a position estimate by integrating the INS velocity components. Hence, the aircraft can continue the landing approach, although the system provides degraded position estimates.

Control Functions

The aircraft attitude control system drives the aircraft control surface to maneuver in pitch and roll as commanded by either the guidance equations or the pilot's sidestick controller.

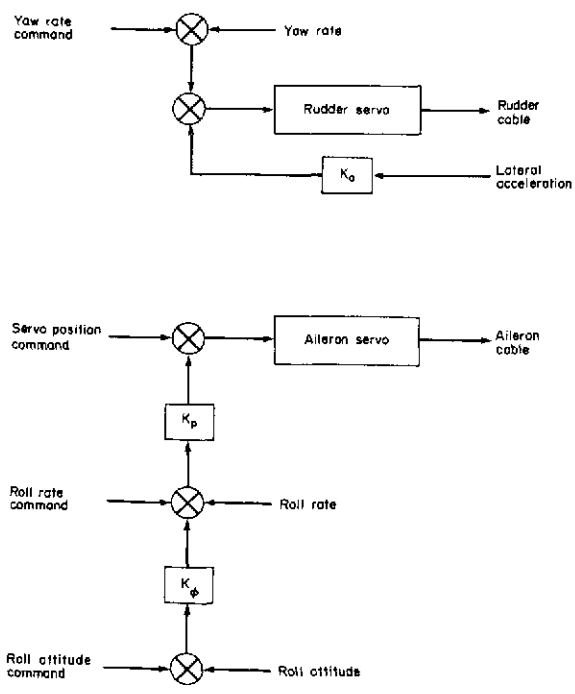

Sketch (d)

Lateral control– The lateral control system consists of a yaw damper and turn coordinator, and a roll-attitude-stabilization loop as shown in sketch (d). The yaw damper drives the rudder servo proportional to the aircraft yaw rate, and the turn coordinator drives the rudder servo proportional to lateral body axis acceleration and a yaw-rate command proportional to aircraft inertial velocity and bank angle. The rudder servo connects directly to the pilot's rudder control cables.

The roll-stabilization loop drives the aileron servo proportional to the differences between roll rate command and roll rate, roll-attitude command and roll attitude, and a feed-forward position command (servo-position command). The feed-forward term and the roll-rate command are zero when the aircraft is under control of the automatic guidance. When the pilot is controlling through the sidestick, however, these terms are proportional to the sidestick lateral displacement as shown in sketch (e). The aileron servo connects with the pilot's aileron-spoiler control cables.

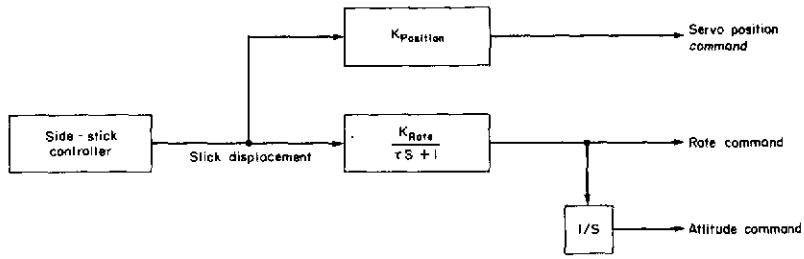

Sketch (e)

Pitch control– The pitch control system consists of a stabilization loop and an automatic trim network as shown in sketch (f). The pitch servo, which is connected to the pilot's elevator control cables, is driven proportional to a feed-forward position command (servo-position command), the difference between pitch rate and commanded pitch rate, and the difference between pitch attitude and commanded pitch attitude. As with the lateral channel, the feed-forward term and the pitch-rate command are zero when the aircraft is under control of the automatic guidance. When the pilot is controlling through the sidestick, these three terms are proportional to the sidestick longitudinal displacement in a manner identical to the lateral sidestick displacement shown in sketch (e). Roll and pitch rate are commanded proportional to the displacement of the sidestick. When the stick is returned to its spring-centered detent position in either axis, zero attitude rate is commanded in that axis and the existing aircraft attitude is maintained.

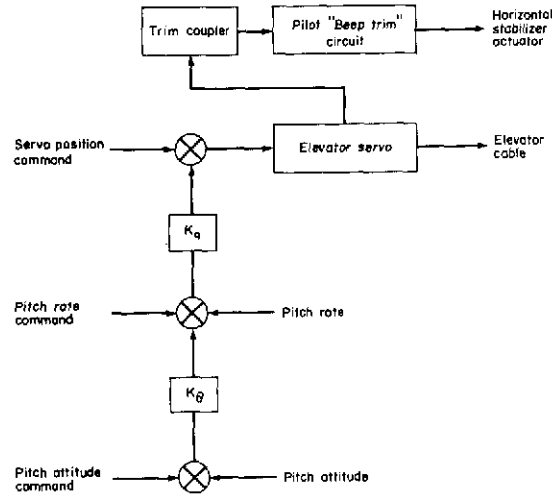

Sketch (f)

The automatic trim circuit is illustrated in the upper part of sketch (f). The CV-990 elevator servo is force limited, and an automatic trim circuit acts to alleviate this force to maintain elevator pitch control. The automatic trim network drives the horizontal stabilizer to aerodynamically align with the elevator and thus decrease the force load on the elevator servo. The simulated shuttle configuration requires a higher stabilizer trim rate than is normally available with the CV-990 autopilot mode. This faster rate is available with the pilot's "beep" trim circuit. The trim coupler shown in sketch (f) senses the load on the elevator servo and pulses the pilot's "beep" trim circuit to move the horizontal stabilizer at a rate proportional to the pitch servo force load. In this way, a proportional autopilot trim rate is available and can vary between zero and the maximum trim rate.

EQUIPMENT DESCRIPTION

CV-990 Aircraft

The NASA CV-990 aircraft is a four-engine jet transport of the approximate size and weight of the Space Shuttle orbiter. The aircraft is equipped with conventional ailerons and spoilers for lateral

control and a rudder for directional control. The spoilers may be symmetrically activated to act as speed brakes. Space Shuttle aerodynamics are approximated by deploying the CV-990's landing gear and spoilers and throttling the engines back to idle at the beginning of an approach. This procedure for simulating Space Shuttle aerodynamics is discussed in detail in appendix A, Matching Shuttle Aerodynamics. Figure 4 shows the overall dimensions of the CV-990, and figure 5 is a photograph of the aircraft during a simulated shuttle approach.

Simulated Shuttle Flight Test System (SS-FTS)

The SS-FTS is an airborne guidance, navigation, and control system that interfaces to existing CV-990 instrumentation. The navigation, guidance, and control functions described in the preceding section are achieved through an experimental automatic control system, which integrates a variety of conventional sensors, special displays, input devices, and control servos with a general-purpose digital computer. The system provides NASA with a flexible research facility for inflight evaluation of Space Shuttle control concepts.

The research test pilot operates the SS-FTS from the copilot's station, which is equipped with special system displays and panels in addition to a side stick hand controller for manual operation in a flight director mode. Through the various panels and displays, the research pilot may operate the system in either the Space Shuttle Vehicle (SSV) mode or the CV-990 autopilot mode. The SSV provides for flight test of Space Shuttle guidance, navigation, and control concepts, while the CV-990 autopilot mode provides the full range of conventional transport modes. The CV-990 autopilot modes include altitude select, altitude hold and vertical speed hold, heading select, VOR navigation, inertial navigation, and autoland.

The system block diagram of figure 6 shows the primary subsystems – the sensors, data adapter, digital computer, control and display devices, and the data recording system. Reference 13 provides a detailed discussion of each of these components, their function, and their operation; a brief review is given here.

Sensors– The sensors determine aircraft attitude, attitude rate and accelerations, position, and position rate and accelerations. The sensors include radio navigation receivers (VOR, ILS glide slope, localizer, and DME), radio altimeter, inertial navigation system (INS), and central air-data system (CADS). The specific instruments used on the CV-990 SS-FTS program and their characteristics are listed in table 1.

Data adapter– The data adapter provides for information transfer between the different subsystems, sensors and displays, and the digital computer. It provides the necessary signal conditioning for all associated equipment. The interface between the computer and the data adapter is a fast, parallel, full party-line transmission system. The data adapter provides multiplexed analog-to-digital, digital-to-analog, and digital-to-digital conversions.

Digital computer– The Sperry 1819A is a general-purpose, airborne digital computer in which the guidance and control laws are programmed and solved in accordance with the sensed inputs to provide signals that drive the control and display systems.

Power control unit– A power control unit provides the interface between the digital computer (via the data adapter) and the control surfaces of the aircraft. It consists of the servo amplifiers required to drive the aircraft surfaces in all three axes, the trim coupler electronics, and relays to drive the trim solenoids, and the yaw damper electronics. The computer, data adapter, and power control unit, were housed in an equipment rack (fig. 7) located in the passenger cabin of the aircraft.

Control and display devices– The system control and display devices (fig. 8) are located for easy accessibility by the research pilot in the right-hand seat. The standard instrument panel was modified to accommodate the installation. The system control and display devices include the mode select panel, data entry panel, status panel, approach progress display, flight director attitude indicator (FDAI), and sidestick controller.

The pilot uses the mode select panel to select the various system modes for both the simulated shuttle test program and the conventional CV-990 operation. The data entry and status panels provide the capability to input data to the computer. The status panel also provides an alphanumeric readout for display of computer inputs through the data entry panel and outputs from the computer, and contains the pushbutton switches for conducting the preflight tests.

The approach progress display provides visual annunciation of the critical submodes of the system. Light progression is from left to right as the approach is made. The ten lights on the right of the panel are associated with the SSV trajectory; the six lights on the left are used with the CV-990 configuration. A panel test button on the upper right provides for inflight testing of the approach progress annunciation circuits from digital computer to the panel. A dim button is provided on the lower right to dim the display for nighttime operation.

A flight director provides the usual cross-pointer flight director display. In addition, a master system warning light on the upper left of this instrument indicates that the pilot should check the status panel for a message – for example, notice of a system or sensor failure or notice for some pilot action such as a change in radio frequency.

The sidestick controller allows the pilot to operate the system in the manual or flight director mode; for manual operations, the computer processes sidestick commands in response to pilot inputs about the roll and pitch axes.

Airborne data acquisition system– Data recording is accomplished onboard the aircraft by the Airborne Digital Acquisition System (ADDAS). The ADDAS (fig. 9) incorporates a Hewlett-Packard 2116B computer, a 2150B Extender Unit, and a variety of peripheral devices that make it a very flexible system. ADDAS accepts data from the 1819A data adapter, a time-code generator, an inertial navigation system, the aircraft surface-position transducers, and other sources. The raw data are recorded on IBM/360 compatible magnetic tape. The data can be acquired, reduced, recorded, and displayed in real time for use during the flight. A preselected number of data measurements may be displayed in engineering units on the high-speed line printer and on the eight-channel strip recorder, allowing "quick look" evaluation while the flight is in progress.

Figure 10 is a cut-away view of the CV-990 showing the relative location of the system components – the navigation aids, the vehicle sensors, and the ADDAS.

Ground-Based Measurement Systems

The simulated shuttle approaches were performed at Edwards AFB on runway 22. The range operations for these tests were controlled by NASA/Flight Research Center (FRC) staff, who coordinated clearances with the traffic control tower and support from the range-operated tracking facilities.

Figure 11 is a diagram of the radio communication links and the ground-based measurement systems. The range systems outlined below were used.

C-band radar (AN/MPS-19C)– The NASA/FRC MPS-19C radar provided long-range tracking of the aircraft. The radar would normally acquire the aircraft (equipped with C-band transponder) at the initiation of the test period and track continuously throughout the test. A real-time plot board display of aircraft position was generated in the FRC control room. These plots were used for quick-look trajectory information after the test flight. Radar tracking data were recorded on digital magnetic tape from the initiation of each approach at 11,300 m (37,000 ft) altitude through to touchdown.

Bell radar– The Bell radar system is a self-contained mobile unit, operated by NASA/ARC and deployed at Edwards AFB to support the CV-990 shuttle flight tests. The facility was used primarily to determine touchdown position data in real time. The Bell radar operator normally acquired the aircraft (equipped with a radar reflector) on the approach just prior to first flare and tracked it through touchdown. The moment of touchdown for each landing was determined by an observer at the radar site. Information on aircraft position and local wind speed and direction was displayed in the Bell radar van. Immediately following each touchdown, the position of the aircraft at touchdown and the local wind conditions were transmitted via radio, to the experimenter onboard the aircraft. This information was used in real-time evaluation of the flight test system performance.

Takeoff and landing facility (TOL)– The TOL facility, operated by the Air Force, was the source of high-accuracy position and velocity data during terminal approach and landing (ref. 14). The facility consists of two towers, each equipped with two Askania cinetheodolites and positioned near each end of the runway. Each tower has an uninterrupted view of the landing aircraft. The cinetheodolite operators normally acquired the aircraft as it passed over the approach end of the runway at an altitude of approximately 45 m (150 ft), and tracked it through touchdown. The TOL data were recorded at four (4) frames/sec in the form of photographic records, which required postflight manual read-up and computer processing to derive position and velocity information.

Time synchronization– Time synchronization was required between the aircraft and the ground tracking facilities to ensure proper correlation of airborne and ground data. The EAFB range continuously transmitted via UHF an IRIG B time-code signal, which was synchronized with WWV. Time-code generators located at each of the ground tracking support facilities (i.e., MPS-19 radar, TOL facility, and Bell radar) were synchronized to the range time. An airborne time-code generator located in the CV-990 aircraft was synchronized with WWV prior to each mission and adjusted inflight when in the vicinity of Edwards AFB. At the end of the day's activities, the synchronization was again checked to determine drifts that occurred during the mission. Through this process, ground and airborne measurements were correlated within 1 msec.

RESULTS AND DISCUSSION

The following section is divided into four subsections: (1) procedures and measurements, (2) guidance performance, (3) navigation performance, and (4) pilot observations. The performance data are presented at selected positions at the beginning or end of each phase of the approach starting with the energy management and proceeding through steep glide slope, shallow glide slope, and touchdown. The data at these selected positions are presented in the form of a Y–Z plot (guidance and navigation window) of system position error from a nominal or reference. Data also are presented in the form of time histories, histograms, and trajectory plots.

Procedures and Measurements

The objectives of the flight tests conducted at Edwards AFB were to demonstrate and evaluate the performance of automatic navigation, guidance, and control system concepts during simulated Space Shuttle approaches and landings.

Fifty-six hours of flying were completed during three test series in June, August, and October-November 1972. The system concept was functionally tested in both an automatic and a manual flight director mode. Fifty-two automatic approaches and landings and eight manual flight director landings were conducted during the course of the three test series. Insufficient data were obtained for evaluation of the manual mode of operation; this report therefore deals only with the results obtained from the automatic mode of operation.

An acceptable set of system gains was established part way through the third test period. The data presented and discussed in this section are from a set of 36 automatic approaches and landings conducted during the latter stages of the third test period. The system gains were invariant for these 36 runs.

Coordinate system– All data presented in this report are referenced to a right-hand Cartesian coordinate system with the origin on the centerline of runway 22 (Edwards AFB), at the ILS glide-path intersection point (GSIP). This coordinate system, known as the runway coordinate system (RCS), is shown in figure 12.

Guidance and navigation windows– Figure 12 shows the three guidance and navigation windows for which system performance data are presented. These windows, all of which are located above an extension of the runway centerline (X axis), are the steep glide-slope-capture window located at $X = -39{,}200$ m (128,600 ft) ($H \cong 6{,}100$ m (20,000 ft)); the first flare window located at $X = -7{,}160$ m (23,500 ft) ($H \cong 457$ m (1500 ft)); and the final flare window located at $X = -487$ m (1600 ft) ($H \cong 21$ m (70 ft)).

Guidance and navigation error– The terms *navigation error* and *guidance error* are represented in figure 13, which shows a ground plane projection of the actual reference trajectory geometrically referenced to the RCS origin (GSIP) and the estimated reference trajectory generated by the system on the aircraft. The difference between the estimate and actual reference trajectory is caused by measurement errors (bias and random noise) in the radio/inertial navigation system. The actual

position of the aircraft at any time is determined by ground-base tracking radar and differs from the position estimated by the onboard system by the magnitude of the navigation error. The navigation error is defined as the time-correlated difference between the ground-based measurement of position and the onboard estimate of position. Analytically, this error is expressed as:

$$\epsilon_N = \sqrt{(X_R - \hat{X}) + (Y_R - \hat{Y}) + (H_R - \hat{H})}$$

The guidance error is determined solely from data computed on board the aircraft. An estimate is made for both the position of the aircraft and the position of the reference trajectory. The guidance error is defined as the time-correlated difference between these two estimates. Analytically, this error is expressed as:

$$\epsilon_G = \sqrt{(\hat{X} - X_{ref}) + (\hat{Y} - Y_{ref} + (\hat{H} - H_{ref})}$$

Guidance Performance

The SS-FTS guidance performance data were recorded during a series of 36 automatic approaches and landings of the CV-990 simulated shuttle vehicle. Eight of the runs were initiated from approximately 11,300 m (37,000 ft) altitude, and the remaining 28 runs from 7,620 m (25,000 ft). The high-altitude approach comprises the energy-management phase, two-segment approach, final flare, and touchdown. Trajectories starting at the lower altitude omit the energy-management portion and initiate the approach in a direction inbound to the runway (straight-in approach).

Performance data from all 36 approaches are presented in the form of summary plots for each approach phase other than the energy management phase – that is, the steep glide slope, first flare, shallow glide slope, final flare, and touchdown.

Energy management phase– Figures 14(a) and 14(b) show two different trajectories of the aircraft from initialization of the descent until capture of the steep glide slope. Each approach starts at a different position within the energy window; the trajectories are designated as E and H for convenient reference (start positions are shown in fig. 2). The upper half of each figure is a downrange-crossrange (X versus Y) plot of aircraft position; the lower half is the corresponding altitude-downrange (H versus X) plot. Each figure shows two paths: the reference path (segmented line) of the aircraft as computed by the onboard guidance program, and the position of the aircraft (continuous line) as estimated by the onboard system. The time-correlated difference between these two paths is the guidance error of the system.

The trajectory E approach begins south of the runway centerline (point A, fig. 14(a)), well within the energy window with the aircraft heading north and closing on the R-zero circle. The aircraft acquires the R-zero circle just prior to crossing the extension of runway centerline (point B), banks right and tracks the R-zero circle. About 50 sec later, the aircraft acquires the outbound radial (point C), banks level, and tracks outbound for about 15 sec. The final turn is initiated (point D) when the altitude predicted to be lost during the turn would result in interception of the extension of the steep glide slope. The control system initially commands a 35° bank

angle, but this bank command rapidly increases to the guidance system bank angle limit of 45° as the inertial velocity increases during the turn, due to the 40 knot tail wind. The bank angle constraint restricts the aircraft from making the required correction and precludes any possibility of following the reference path. The aircraft drifts to the left of the path but recovers during the latter part of the turn as the aircraft heads into the wind. The turn is completed on the runway centerline at about 7,000 m (23,000 ft) altitude (point E) with the steep glide slope acquired slightly above 6,100 m (20,000 ft) (point F).

During the initial run-in to the R-zero circle, the guidance error is small; during the final turn maneuver, the guidance error becomes more pronounced as the aircraft consistently drifts to the left of the reference path. The maximum guidance error during the approach, 1580 m (5200 ft), occurred about half way through the final turn.

System performance for a low-energy condition, trajectory H, is presented in figure 14(b). The approach begins north of the runway centerline and appears to be within the energy window close to the boundary (point A). Due to INS drift, the onboard estimate of the aircraft position is displaced from the actual initiation point (from radar) by about 1.5 n.mi. At initiation, the aircraft is off by 30° to the right in heading and low on initial velocity (M = 0.80). After the navigation system is updated via the radio NAVAIDS (DME-DME), the aircraft corrects the position estimate and heading error, starts closing the range to the R-zero circle, and acquires the circle about 30 sec later (point B). The R-zero circle is tracked for about 2.5 min while the aircraft, flying close to maximum L/D, descends at 1220 m/min (4000 ft/min). At the intercept of the outbound radial (point C), a low-altitude (energy) condition exists. The system skips the outbound radial phase, immediately proceeds into the final turn (point D), and attempts to make a minimum radius turn. During the turn, the aircraft drifts left of the desired path due to the winds and the bank-angle limit. For the entire approach, the aircraft altitude is lower than desired and at completion of the final turn (point E), the aircraft is 457 m (1500 ft) below the steep glide slope. Remaining in the operational L/D mode, the aircraft intercepts and captures the steep glide slope at an altitude of 5,340 m (17,500 ft) (point F). Interception of the steep glide slope at an altitude below 6,100 m (20,000 ft) resulted from a combination of errors in velocity, heading, and altitude, at initiation of the run (point A).

Guidance error at steep glide-slope-capture window– The guidance errors at the steep glide-slope-capture window (X = -39,200 m (128,600 ft); H ≅ 6,100 m (20,000 ft)) for all the high-altitude runs are shown in figure 15. At this window location, the guidance error is zero if the aircraft is on the computed runway centerline and on the computed steep glide-slope beam at 6,100 m (20,000 ft) above ground level.

Eight runs are shown in this figure, although only four represent approaches where the system has actually captured the steep glide slope. For these four runs (indicated by the symbols *without* the flags), the vertical errors are less than 50 m (160 ft) and the lateral errors less than 1500 m (4900 ft). The large lateral errors result from the guidance system bank-angle limit, which makes it impossible to correct for the effect of high-altitude winds. As previously noted, the bank-angle limit of 45° is rapidly saturated during the final turn maneuver when high winds are encountered.

For the remaining four runs (indicated by the symbols with the flags) the pitch guidance is still in the operational L/D mode.

Steep glide-slope tracking– Figure 16 shows the tracking performance of the system during the steep glide-slope phase of the approach. The shaded regions represent the envelopes of maximum vehicle excursions for the series of 36 automatic approaches. The vertical tracking error relative to the 10° glide slope is shown in the upper part of the figure. The lateral tracking error relative to the center of the ILS localizer signal is shown in the lower part of the figure.

The solid trace within each shaded region is a time history of guidance errors for one specific run that is considered to be an example of "good tracking performance." Note that while lateral guidance errors may be larger than 150 m (490 ft) at steep glide-slope capture, they converge to relatively small values (< 24 m (78 ft)) prior to first flare.

Guidance error at first flare window– Figure 17 shows the guicance error measured at the first flare window (X = −7,160 m (23,500 ft); H ≅ 457 m (1500 ft)). In this case, the reference is the center of the ILS localizer signal and the center of the steep glide slope as computed by the navigation equations using a single DME and the barometric altimeter.

In essence, these data indicate the effectiveness of the guidance and control system in maintaining the aircraft on the desired flight path. If the guidance errors were zero, the data points would be clustered on the estimated glide-slope centerline, which is the origin of the graph. For these data, the vertical mean error is zero with the lateral mean error 3.1 m (10 ft) to the left. The 1σ error about the mean is ±6.1 m (20 ft) in the vertical direction and ±9.2 m (30 ft) in the lateral direction.

First flare altitude– The altitude at which the first flare occurred is presented in figure 18. In this histogram, the height of the vertical bar indicates the number of times the aircraft initiated the flare maneuver within a given altitude zone. Each altitude zone is 5 m (16 ft) in height. For example, the aircraft initiated flare 15 times in the zone between 440 m (1444 ft) and 445 m (1460 ft) altitude. Nominally, the aircraft would initiate first flare at a point 0.97° above the center of the 2.5° glide-slope beam, which corresponds to an altitude of 427 m (1400 ft) for the nominal flight path. The data indicate that the mean first flare initiation altitude was 441 m (1450 ft) above the ground (a bias of +14 m (46 ft)) with a 1σ dispersion of ±10.2 m (34 ft). In terms of the ILS glide-slope-beam parameters, the errors correspond to a beam bias of +0.08° and a random error of +0.05°, which errors can be attributed to the ground-based ILS transmitter or the airborne receiver or both. No in-depth study was made to identify the source of the error, although a separate analysis of the Edwards AFB ILS beam characteristics (unpublished) indicated that the day-to-day variation of the glide-slope-beam elevation angle could be as large as ±0.2°.

Speed control– Figure 19 shows the speed variations during the approach from 11,300 m (37,000 ft) to touchdown for trajectories E and H. The aircraft velocity is not controlled directly but converges to a constant calibrated airspeed for a particular angle (or L/D). During the period from initiation of the approach until steep glide-slope capture, the aircraft is controlled to fly in the operational L/D mode. The L/D is essentially constant at a value slightly less than the maximum L/D for the shuttle. The aircraft pitch attitude is controlled to maintain this L/D. During the descent, the velocity should remain constant at about 230 knots (CAS) until steep glide-slope capture.

At steep glide-slope capture, the simulated shuttle pitched over to fly a −10° glide path during the steep glide-slope segment. The velocities for each trajectory should have converged toward the nominal value of 305 knots, although exact convergence was precluded in practice by atmospheric

wind and the inability to precisely set up the aircraft configuration to obtain the desired L/D. The aircraft configuration was set up at the initiation of the approach and consisted of landing gear down, throttles in flight-idle position, and speed brakes deployed. The speed brake setting was different for each approach and was chosen to compensate for changes in the aircraft weight as the tests progressed. An incremental 5° change in speed brake was made for each 9,080 kg (20,000 lb) change in aircraft weight. A 5° error in the speed brake setting can result in an error as large as 15 knots (CAS) in the equilibrium velocity.

This speed brake law is a simple approximation that gives acceptable results. A refined speed brake deployment technique using a stored nominal velocity profile and modulated speed brakes could converge all velocities at first flare and landing to within a very narrow dispersion. Using the simple speed law which was implemented, the velocity dispersions at first flare were large but acceptable. Figure 20 presents the velocity-dispersion data at nominal first flare in the form of a histogram of velocities versus number of occurrences. The figure shows that the mean velocity for 36 approaches was 290 knots (CAS) with a 1σ dispersion of ±10 knots.

A final speed brake adjustment was made just prior to first flare (≅ 760 m (2500 ft)) to compensate for atmospheric winds and error in initially setting the configuration L/D. This setting is a function of the existing atmospheric winds as measured by the onboard INS. No further speed brake adjustments were made during the remainder of the approach to touchdown. Velocity dispersions at final flare and landing are presented later.

Shallow glide-slope tracking— The guidance system performance during the first flare and shallow glide-slope modes is shown in both the vertical and horizontal plane in figure 21. The three flight paths are from three landing approaches; two represent the maximum excursions about the ILS glide-slope beam, and the third represents a nominal path. The dispersions are caused primarily by the variation in first flare initiation altitude. As previously noted, the flare mode is engaged when the aircraft descends to a point that is 0.97° above the ILS glide slope. Since the ILS receiver signal is used directly to measure this displacement, the flare initiation altitude varies as a function of the noise on this signal. Variation of ±0.2° were detected in the glide-slope-beam deflection. The first flare began at about 463 m (1519 ft) altitude for the upper path in figure 21, at about 431 m (1414 ft) for the middle path, and at about 415 m (1361 ft) for the lower path.

The variation in the first flare performance affects only the initial tracking performance of the shallow glide-slope mode. The vertical errors from the ILS glide-slope beam after shallow glide-slope mode engagement are reduced to less than 8 m (26 ft) at an altitude of 100 m (328 ft); below this altitude, tracking errors remain less than 8 m.

In the horizontal plane, the system is in the runway centerline tracking mode, which is a continuation of the same guidance mode used during the steep glide-slope phase.

During the shallow glide-slope tracking phase, the lateral guidance errors decrease as the aircraft approaches the runway as shown in figure 21.[1] This reduction is confirmed by comparing

[1]Note that the lateral profiles shown in figure 21 correspond to the vertical profiles presented in the same figure, but they do not necessarily indicate the maximum excursions that occurred in the lateral plane when all approaches are considered.

the lateral guidance error at the first flare and the final flare windows (figs. 17 and 22), where the standard deviation of the error reduces from ±9.2 m (±30 ft) to ±3.5 m (±11 ft). The primary cause for this effect is the error in the lateral position estimate. The noise in the lateral position estimate is proportional to the product of the localizer beam angular noise and the aircraft distance from the localizer antenna. If the angular beam noise has a constant level, the lateral position estimate error will decrease as the aircraft approaches the runway. The ratio of distance between the aircraft and localizer antenna at the final flare window to that of the first flare window is 0.44, and the ratio of the lateral error standard deviation at the final flare window to that of the first flare window is 0.37. Hence, the change in distance accounts for a substantial part of the lateral guidance error reduction.

Guidance errors at final flare window– Figure 22 shows the system guidance performance at the final flare window (X = 487 m (1600 ft); H ≅ 21.4 m (70 ft)). The reference is the center of the ILS localizer beam and the ILS glide-slope beam.

The mean of the vertical error shown in figure 22 is 2.1 m (7 ft) above the glide-slope centerline; the standard deviation of the vertical error is ±2.5 m (8.2 ft). The CV-990 entered the ground effect about 31 m (102 ft) above the ground, which tended to increase the effective lift, thereby arresting the sink rate. This tendency to float above the glide slope prior to final flare was also observed in the radar tracking data.

The mean of the lateral guidance error is zero, which means that on the average the aircraft is tracking the center of the ILS localizer beam. The standard deviation is ±3.5 m (11 ft).

Final flare initiation– The altitude and altitude rate at which final flare is initiated is presented in figure 23. Flare initiation should occur when the altitude above the ground equals 9.2 m (30 ft) plus twice the altitude rate (i.e., $H = 9.2 + 2\dot{H}$). The straight line angling upward to the left in figure 23 maps the points in the H-versus-$\dot{H}$ phase plane where the final flare should be initiated. The points at which the flares were actually initiated for the 36 approaches are shown clustered about this line. Nominally, the aircraft would be descending at about 4.5 m/sec (15 ft/sec) at final flare initiation at 18.3 m (60 ft) altitude. The mean altitude rate and altitude from these data are 3.9 m/sec (12.8 ft/sec) and 16.8 m (55.1 ft), respectively. The standard deviation of the data is shown in the form of a 1σ dispersion ellipse represented by the shaded area.

Speed dispersions at final flare– The histograms of calibrated airspeed and ground speed at final flare initiation are shown in figure 24, which plots the magnitude of the velocity versus the number of occurrences within each 5-knot velocity zone. For the 36 approaches, the mean velocity is 184 knots for the calibrated airspeed and 189 knots for ground speed with standard deviations of ±8 knots and ±15 knots, respectively.

Position dispersions at touchdown– Figure 25(a) presents the position dispersions of the aircraft at touchdown for 36 automatic landings. These data are presented as histograms, with the height of a given vertical bar indicating the number of times the aircraft touched down in a given zone on the runway. Distance along the centerline of the runway is divided into 50-m (164-ft) zones.

The zero position is the glide-slope intercept point (GSIP) on the runway. The mean touchdown point was 251 m (823 ft) beyond the glide-slope intercept point with a 2σ dispersion of

±325 m (1065 ft); in other words, approximately 95 percent of the landings were contained within a zone 650 m (2130 ft) long. For comparison, the FAA Category II 2σ criterion for distribution of touchdown for certification of commercial transport autoland systems is shown as the shaded zone. The FAA Advisory Circular (ref. 15) specifies that 95 percent of the landings are to be in a zone 457 m (1500 ft) long.

Across-the-runway, or lateral, disperions are shown in figure 25(b). The runway centerline is taken as zero, and zones across the runway are defined at 2-m (6.6-ft) intervals. The 2σ dispersion is ±8.4 m (±28 ft) compared with the FAA criteria of ±8.2 m (±27 ft). The centerline of the ILS localizer beam at Edwards AFB was biased to the right side of the runway centerline; this localizer offset was removed from the lateral dispersion data in figure 25(b) to give a more realistic picture of the system performance with a true Category II ILS. The magnitude of the ILS bias is apparent in the data on navigation errors at the first flare and final flare windows.

Speed dispersion at touchdown– The histograms of vertical speed, calibrated or indicated airspeed, and ground speed at touchdown are shown in figure 26, where the magnitude of the parameter is plotted versus the number of occurrences.

The design vertical speed at touchdown was 0.61 m/sec (2 ft/sec). A mean vertical speed of 0.52 m/sec (1.9 ft/sec) was obtained during the flight tests.

The system was designed to achieve a calibrated airspeed (CAS) at touchdown of 175 ± 25 knots. The guidance system has indirect (open-loop) control of the CAS through an adjustment of the speed brake at first flare and attempts to minimize the variations in CAS at touchdown. The flight test data show a mean of 166 knots and a range of ±24 knots ($\sigma = \pm 9$ knots). A function of local wind conditions, the expected larger ground speed dispersion at touchdown is indicated ($\sigma = \pm 16$ knots). The mean value for the ground speed was 174 knots.

The ground winds during these flights varied from a low of zero to a high during one approach of 30 knots but generally remained under 10 knots. The average winds for all runs had a headwind component of 7.6 knots and a crosswind component of 1.1 knots.

Navigation Performance

The onboard navigation system uses the available measurements from radio navigation aids (DME, VOR, ILS) and onboard instruments (INS, Baro, and radio altimeter) to provide estimates of the present aircraft position and velocity. Direct ground-based measurements (MSP-19 tracking radar) of these parameters are taken as the standard (indicating the actual aircraft position) and compared with the onboard measurements to determine the performance of the onboard system. System performance data are presented and discussed for each of the three navigation windows (steep glide-slope capture, first flare, and final flare). In addition, a trajectory plot and corresponding time histories of navigation errors are presented for one example of a high-altitude approach from 11,300 m (37,000 ft) to touchdown.

Approach trajectory– The trajectory of the aircraft during the energy-management phase and continuing until touchdown is presented in figure 27(a). The top half of the figure shows the downrange-crossrange position of the aircraft as estimated by the onboard system and measured by

the ground-based tracking radar. The lower half of the figure presents the corresponding altitude-downrange plots. The time-correlated difference between the two trajectories in each figure is the navigation error of the onboard system. The time histories of these navigation errors are shown in figure 27(b).

The onboard system was initialized about 1 min prior to start of the approach on INS only. The INS drift was not significant, and the tracking radar indicated a position within 1000 m (3280 ft) of the onboard computed position. As the radio navigation data are introduced, the system updates the position estimate until at the start of the approach (point A, fig. 27(a)), the onboard estimate agrees within 300 m (980 ft) of the position determined by radar. Note that as the aircraft proceeds on the approach, the estimate trajectory (X–Y plane) is displaced slightly to the west of the radar-measured trajectory. This offset of approximately 300 m (980 ft) is constant throughout the energy-management phase. The offset probably results from a bias in the slant range measurement to the No. 2 DME station (George AFB), which is located east of the approach. An error in the designated location for the station or a bias in the DME transmitter/receiver could cause the translation in the trajectory. With the data available, it was not possible to state with certainty the source of the error.

The altitude range plot also shows a discrepancy between the radar and onboard altitude measurements. This error was fairly constant at about 150 m (490 ft), down to an altitude of 9,000 m (29,500 ft). After initiation of the final turn (point D), the error disappeared rather abruptly. Analysis of the data showed that this strange behavior could be attributed to the tracking radar. At about 2 min into the approach, the radar elevation angle took an incremental jump of 0.2° within a 2-sec period. The onboard estimates of altitude decreased smoothly through this region with no apparent anomalies.

Figure 27(b) shows the difference between the onboard estimate of position ($\hat{X}$, $\hat{Y}$, $\hat{H}$) and the MPS-19 ground radar measurement of position (X_R, Y_R, H_R) as a function of time from the start of the approach through to touchdown. Significant events are labeled for comparison with figure 27(a). The total navigation errors shown in each trace reflect a combination of errors due to ground navaid/airborne receiver signal bias, off nominal atmosphere effects, possible time skews between airborne and ground data, and the basic navigation system errors resulting from software/hardware mechanization.

The trajectory offset referred to above is apparent in both the X- and Y-error time histories. The vector sum of the X and Y errors is consistently about 300 m (980 ft) until localizer capture at point E, after which the errors converge rapidly and remain acceptably small($<$100 m (328 ft)) during the steep glide-slope portion (points F and G). At first flare, the X and Y errors are 15 m (50 ft) and 18 m (60 ft), respectively. At touchdown, the lateral navigation error is about 11 m (36 ft). Since the deviations from the ILS localizer and glide slope are the primary navigation inputs after flare, the longitudinal navigation error (X_{err}) has no significance and is not shown.

The time history of the altitude error (H_{err}) shows errors as large as 150 m (490 ft) during the first 2 min of the approach. The error then abruptly decreases to small values ($<$ 50 m (160 ft)), remaining close to zero throughout the steep glide-slope portion and becoming essentially zero at touchdown.

Navigation error at steep glide-slope capture– Figure 28 shows the navigation error at the steep glide-slope capture window (X = −39,200 m (128,600 ft); H ≅ 6,100 m (20,000 ft)). At this window, the aircraft nominally was on the runway centerline extension and had just completed or was about to complete the steep glide-slope capture. With the system navigating in the DME/DME mode, the standard deviation of the total expected position measurement error (vector sum of X_{err}, Y_{err}, and H_{err}) as determined from analysis of the raw DME signals and Baro-altimeter signal is ±457 m (1500 ft). On incorporation of inertial blending, the navigation system reduced this error to an estimation error having a standard deviation of ±94 m (308 ft) for the data shown in figure 28. The biases in lateral error of −97 m (−318 ft) were the result of either biases in the onboard navigation receivers or uncertainty in the location of the VOR/DME stations. The VOR/DME locations were obtained from the IFR-Supplement, United States Effective 9 Dec 1971 to 1 Jan 1972, which lists such locations to an accuracy of 1 sec of arc (≅30 m (98 ft)). The bias in the altitude error is +47.5 m (156 ft) and can be accounted for predominately as the effect of nonstandard atmospheric conditions.

Navigation error at first flare window– Figure 29 shows the difference between ground-measured (radar) aircraft position and the onboard aircraft position estimate as the aircraft passes through a window positioned at the initiation of first flare. The aircraft is nominally at an altitude of 457 m (1500 ft), on the steep glide slope, and on the runway centerline extension 7,160 m (23,500 ft) downrange from the RCS origin. The navigation system is in the DME/localizer mode.

The data show that the aircraft is off to the right of the runway centerline extension for all runs and below the glide-slope beam for all but one run. This consistent offset is due to the fact that the ILS localizer beam bends to the right of the runway. The beam position was measured at the touchdown point on a daily basis during the flight test and its position was found to correlate with the bias shown in this figure. The reason for the aircraft being below the glide-slope beam is not explained. Previous studies have shown that the standard deviation of the total expected measurement error (one DME range, ILS localizer deviation, Baro-altimeter) at the first flare window is ±107 m (350 ft). The standard deviation of the total navigation error from the data presented here is ±16.8 m (55 ft).

The data show interesting groupings from one flight series to the next. For example, the data group to the far right (diamond symbols) were collected during a series of runs made on a single day. These data, as well as previous qualitative observations of the ILS beam, lead one to question the stability of the ILS. It is conjectured that the centerline of the ILS beam drifted significantly from day to day, with the "far right" data group collected on the day when the ILS drift was at an extreme.

Navigation error at final flare window– Figure 30 shows the difference between the ground-measured aircraft position and the onboard estimate at a point 487 m (1600 ft) downrange from the touchdown point. The aircraft is nominally at an altitude of 21.4 m (70 ft) on the ILS glide-slope beam and on the runway centerline. The navigation system is in the localizer/glide-slope mode. Again, the localizer beam is offset to the right, as in figure 29. Previous studies have shown that the standard deviation of the total expected error in the measurement at the final flare window is ±12 m (±39 ft). The standard deviation of the total navigation error for the flight data shown here is ±4.3 m (±14 ft).

Pilot Observations

The simulated shuttle missions were flown by several different NASA pilots and pilots from the U. S. Air Force, North American Rockwell, and the Sperry Rand Corporation. Comments solicited from the individual pilots after the missions are summarized in this section.

Standard aircraft operating procedures for the CV-990 were followed during takeoff and climbout to the test initiation point in the test area. Primary means of navigation during this phase was with the inertial navigation system. Ground-based radar tracking with a voice link was available to give advisory information. A primary piloting task was to arrive at the test initiation point with the proper aircraft altitude and airspeed, and with proper aircraft/system configuration. This required pilot inputs to the system relative to the chosen landing site, the navigation aids to be used, and the aircraft weight.

The pilot and computer communicated via the data entry panel (keyboard) and the status panel (display). The pilot initiated the conversation by depressing the site selection button on the mode select panel. He then entered the appropriate response to the computer display via the keyboard. The computer requested the landing site identification code (i.e., E1 for Edwards AFB), the field barometric pressure, and the aircraft weight. After pilot entry of aircraft weight, the status panel readout the initial speed brake setting, which was manually set by the pilot. Appropriate navaid stations (DME/VOR) were tuned and identified. These signals were inputs to the system to update the position estimates. Failure to obtain valid ground navigation signals did not disrupt operation of the guidance system. In the event of an invalid navaid signal, guidance signals were available based on the INS-only condition until satisfactory navaid signals were restored; the INS-only condition was indicated by a status panel message and a flashing light on the mode select panel. The pilots observed no discontinuities in the flight director display as a result of navaids switching in and out.

Simulated shuttle operation was initiated by selecting the SSV switch position, pressing the AUTO button on the mode select panel, deploying the speed brake and landing gear, and retarding the throttles to flight idle. From this point on, the complete approach through touchdown was automatic, with the exception of a final speed brake adjustment and flap deployment during the last stages of the approach.

The approach progress display annunciated the particular phase of the approach or the mode in which the system was operating. Although this display was much simpler than originally planned for the SSV simulation, the pilots agreed that it was sufficient and provided satisfactory azimuth and elevation flight path orientations. There was never any confusion as to which phase of the profile a pilot was flying or what to expect next.

Throughout the energy-management phase of the approach, the pilot performed continuous cross checks. For example, the INS position was cross checked with a chartered position; and the raw bearing and distance-to-ground navigation aids, displayed on standard cockpit instruments, were used to derive an independent position. Altitude and airspeed were compared with the nominal values as the approach progresses. Tracking radar and a normal communications channel provided an additional position for information relative to the desired track.

As the approach progressed, the pilot workload increased. The final turn into the runway centerline was essentially the same procedure as final ILS localizer intercept during a conventional aircraft approach, except that the inbound track was captured at about 6,100 m (20,000 ft) altitude. The steep glide-slope capture occurred as the extension of the steep glide-slope path was intercepted. The aircraft pitched down to capture the 10° glide path. In this case, the pilots again observed no discontinuity in the flight director signals during transition to the steep glide slope. The pilot had both displacement from the reference path and director information to the reference path. Loss of the radio signal from either the localizer or DME was indicated by a status panel message. When the signal was reacquired, a smooth transition to the updated track was provided by the flight director. As the aircraft passed through an altitude of 762 m (2500 ft), a final speed brake adjustment was annunciated on the status panel and made by the pilot.

The stabilized rate of descent on the steep segment was about 1600 m/min (5200 ft/min). The pilots felt that there was always adequate time to anticipate capture of the ILS glide slope by observing the glide-slope displacement bar, and the pressure and radio altimeters. At first flare initiation, the approach progress display indicated first flare and the flight director commanded a pitch up to capture the shallow glide slope. The first flare maneuver was smooth and predictable. At approximately 245 knots on the shallow glide slope, the status panel displayed the command for flaps equal to 10°. A manual flap setting was made by the pilot. The speed brake adjustment prior to the first flare and the flap setting are both functions that could easily be automated.

The airspeed and altitude were cross checked at several key heights on the shallow glide slope to determine if the velocity was within limits. If conditions were outside these limits, the approach could be aborted. The consistency of the touchdown positions and velocities were remarkable considering the lack of wind compensation and a "ground rule" that prevented using small additional speed brake corrections for speed errors easily detected by the pilots.

Several sidestick controlled landings were completed using the final flare and touchdown guidance signals provided to the pilot on the flight director. Automatic landing data had priority during the flight test, so pilot observations of the manual sidestick mode of operation are incomplete.

While flying in the automatic mode, the pilots wanted to see some positive action by the aircraft at the beginning of final flare, or at least by the time the altitude dropped to 16 m (50 ft). At the high approach speeds, the sink rates prior to final flare were 1.5 times that of a normal approach and there was little time to react to an anomaly. Although the aircraft ground effect produced the major reduction in sink rate at these speeds, it occurs too late for the pilots to comfortably use it as an indicator of flare occurrence. Consequently, the flare guidance was programmed to produce a small but rapid pitchup attitude change at flare initiation, which gave the pilots a reliable indication that the flare had begun.

At about 3 m (8 ft), the decrab mode was entered. No tests were made in high crosswinds. For the low crosswind conditions encountered, however, this mode operated satisfactorily and, in fact, gave the pilots a high degree of confidence in the system as it allowed automatic touchdowns at very high speeds where even small drift angles could produce high side loads.

Touchdown velocities as high as 210 knots were experienced. Although the high touchdown velocities caused some apprehension when first encountered, they still allowed sufficient time to

safely monitor events. These tests demonstrated the acceptability of touchdown velocities as high as 210 knots, and the pilots agreed that the limiting factor at the high velocities was tire strength rather than their ability to monitor the system or control the aircraft.

CONCLUSIONS

Thirty-six automatic approaches and landings were made during an investigation of an automatic approach and landing concepts for a simulated Space Shuttle vehicle represented by the NASA Convair 990 aircraft. The CV-990 was especially equipped with a digital navigation, guidance, and control computer connected to the aircraft control system for automatic flight control, and with displays to allow the pilot to monitor system performance. Results of these limited tests led to the following conclusions:

1. Automatic landing of a Space Shuttle class vehicle are feasible without air-breathing engines.

2. Under the test conditions, the following performance was obtained:

   a. Blended radio/inertial navigation using ILS, VOR, and DME gave 2σ deviations at touchdown of ±325 m (±1065 ft) longitudinally and ±8.4 m (±28 ft) laterally.

   b. The DME/DME Baro-altimeter navigation concept for high-altitude energy management had a total position accuracy of ±94 m (±308 ft) (1σ) at an altitude of 6,100 m (20,000 ft).

   c. The low-altitude guidance concept converged vertical and lateral guidance errors greater than 70 m (230 ft) at an altitude of 6,100 m (20,000 ft) to errors with a standard deviation of ±2.5 m (±8.2 ft) vertically and ±3.5 m (±11.5 ft) laterally at an altitude of 21.4 m (70 ft).

3. The pilots had no difficulty monitoring events with aircraft touchdown ground speeds as high as 210 knots.

4. Simulated shuttle vehicle touchdown data on velocity, descent rate, and dispersion were provided to help define runway size required for the Space Shuttle vehicle.

5. The CV-990 simulated shuttle program demonstrated the satisfactory operation, dependability, and inherent flexibility of a programmable digital flight computer for guidance, navigation, and control of the Space Shuttle in the terminal area approach and landing phases of flight.

Ames Research Center
National Aeronautics and Space Administration
Moffett Field, Calif. 94035, July 10, 1974

APPENDIX A

MATCHING SHUTTLE AERODYNAMICS

Effective simulation of a Space Shuttle mission in the terminal area requires that the aerodynamic characteristics of the test vehicle match those of a typical shuttle configuration. The CV-990 aircraft was studied extensively to determine its suitability for simulations of a Space Shuttle Orbiter in the terminal area. Several years ago, CV-990 flights at Edwards AFB demonstrated low L/D unpowered approaches and showed that the CV-990 was representative of both the size and performance of the proposed shuttle orbiter (refs. 1 and 2). More recently (ref. 4), a detailed examination of the aerodynamic characteristics of the CV-990 for various configurations of flap, landing gear, and speed brake deployment, and comparisons with a candidate Space Shuttle vehicle, showed that the CV-990 has considerable capability for accurately simulating the aerodynamic characteristics of proposed shuttle configurations. Through proper deployment of the speed brakes, flaps, and landing gear, a fairly wide range of prospective L/D characteristics can be matched.

At the time a specific orbiter was to be selected for simulation by the CV-990, shuttle vehicle design was still evolving. The concept chosen corresponded to a high-crossrange configuration (proposed in June 1971) having a maximum subsonic trim L/D of 6.7. The CV-990 aircraft was constrained during the approach to fly the same L/D-versus-airspeed variation as would be flown by the 1971 shuttle vehicle. A match of the CV-990 L/D-versus-airspeed curve provided not only the same flight path angle as the proposed shuttle, but also the same airspeed, speed-stable energy-management response, and therefore trajectory dynamics. The time duration of each phase of the approach from 11,300 m (37,000 ft) to landing was approximately the same as the shuttle.

Figure 31 compares the variation of L/D versus airspeed over the velocity region for the terminal approach of the CV-990 and the shuttle. The operational capability of the CV-990 is indicated by the shaded region, whose shape is defined by limit positioning of the speed brakes and flaps. The landing gear are deployed and the throttles are at flight idle. The envelope was constructed from flight data published in reference 2 and from unpublished data acquired in flight at Ames Research Center (ARC).

The solid line in figure 31 shows the L/D variation for the proposed shuttle orbiter. The dashed lines connect several operating points for the CV-990 during a simulated shuttle approach. The nominal CV-990 approach simulates shuttle operations on the front side (speed stable) of the L/D curve (i.e., at a velocity in excess of that for maximum L/D). Operations in this region preserve the normal piloting techniques (i.e., pitchup decreases flight path angle) and permit limited control for extending the range by pitching the aircraft to maximum L/D.

The geometry of the CV-990 aircraft is fixed at the beginning of the approach and is not changed during the energy-management and steep glide-slope equilibrium glide phases. The configuration is set up to permit a good match of L/D during the steep glide-slope phase. Consequently, the L/D during the energy-management phase is slightly high. The difference in slope between the two curves means that the speed convergence for the CV-990 is more rapid than that of the shuttle

configuration (ref. 9). The convergence time constant of the CV-990 is about half that of the simulated shuttle; consequently, the altitude loss during speed convergence is half as long for the CV-990 (1300 m (4260 ft)) as for the simulated shuttle (2600 m (8530 ft)).

A 10° flap deployment for the CV-990 is required during the terminal phase of the approach (first flare to touchdown). The flaps must be extended to keep the pitch attitude within the operational limits of the CV-990 and avoid tail scrape at landing. In spite of these limitations, the CV-990 as configured is a good match to the orbiter from an L/D standpoint.

The dynamic response characteristics of the CV-990 aircraft are well documented (ref. 16). Although there are certain similarities between the short-period dynamics of the CV-990 and shuttle (ref. 4), no direct attempt was made to model the shuttle short-period response or handling qualities. Thus, it is not suggested that the CV-990 simulates the short-period dynamics of the Space Shuttle. This problem is quite complex and beyond the scope of this study.

REFERENCES

1. Bray, Richard S.; Drinkwater, Fred J., III; and White, Maurice D.: A Flight Study of a Power-off Landing Technique Applicable to Re-entry Vehicles. NASA TN D-323, 1960.

2. Kock, Berwin M.; Fulton, Fitzhugh L., Jr.; Drinkwater, Fred J., III: Low-Lift-to-Drag-Ratio Approach and Landing Studies Using a CV990 Aircraft. NASA TN D-6732, 1972.

3. Osder, S.; Keller, R.: Study of Automatic and Manual Terminal Guidance and Control Systems for Space Shuttle Vehicles. Vol. I, Sections 1–3. NASA CR 114 400, 1971.

4. Osder, S.; Keller, R.: Study of Automatic and Manual Terminal Guidance and Control Systems for Space Shuttle Vehicles. Vol. II, Section 4, Appendix B. NASA CR 114 401, 1971.

5. Osder, S.; Keller, R.: Study of Automatic and Manual Terminal Guidance and Control Systems for Space Shuttle Vehicles. Final Rept. Suppl. NASA CR 114 407, 1971.

6. Cockayne, William; Rusnak, Walter: Study of Automatic Flare and Decrab Guidance and Control System for the Space Shuttle Vehicle. NASA CR 114 436, 1971.

7. Schmidt, S. F.: Precision Navigation for Approach and Landing Operations. 1972 Proceedings of JACC, pp. 455–463 (Stanford University), Aug. 16–18, 1972.

8. McGee, Leonard A.; Smith, Gerald L.; Hegarty, Daniel M.; Carson, Thomas M.; Merrick, Robert B.: Flight Results From a Study of Aided Inertial Navigation Applied to Landing Operations. NASA TN D-7302, 1973.

9. Stapleford, Robert L.; Klein, Richard H.; Hob, Roger, H.: Handling Qualities Criteria for the Space Shuttle Orbiter During the Terminal Phase of Flight, NASA CR 2017, 1972.

10. Edwards, F. G.; Foster, J. D.: Flight Test Results From the CV990 Simulation Space Shuttle During Unpowered Automatic Approaches and Landings. NASA TM X-62,285, 1973.

11. Smith, Donald W.; Edwards, Frederick G.; Foster, John D.; and Drinkwater, Fred J., III: Flight Test of an Automatic Approach and Landing Concept for a Simulated Space Shuttle Represented by the NASA Convair 990 Aircraft. AGARD Symp. on Guidance and Control Panel Meeting(Geilo, Norway), Sept. 24–26, 1973.

12. Gaylor, Randal: Flight Test System for Study of Space Shuttle Vehicle Guidance and Navigation Concepts. Final Rept., Publ. No. 71-0386-00-00, Sperry Flight Systems Div., Phoenix, Arizona, 1973.

13. Hegarty, Daniel M.: A Functional Description of a Digital Flight Test System for Navigation and Guidance in the Terminal Area. NASA TM X-62,400, 1974.

14. Anon.: Air Force Flight Test Center Test Facilities Handbook. Section V, Rept. No. FTC-TIH-63-2003, Jan. 1967.

15. Advisory Circular No. 20-57A, Automatic Landing Systems. Dept. of Transportation, Federal Aviation Admin., 12 Jan. 1971.

16. Gilyard, Glenn B.: Flight-Determined Derivatives and Dynamic Characteristics of the CV990 Airplane. NASA TN D-6777, 1972.

TABLE 1.– PERFORMANCE OF CV-990 SS-FTS AIRBORNE NAVIGATION AIDS AND SENSORS

Description	Manufacturer	Model	Function	Range	Resolution	Accuracy
VHF navigation receiver	Collins	51R-3	VOR	0 to 360°		±1/2°
			LOC	±2°		±0.05°
Glide-slope receiver	Collins	51V-3	GS	±0.7°		±0.028°
Distance measuring equipment	Collins	860E-2	DME	0 to 195 n.mi.		±0.1 n. mi. up to 5 n. mi. ±0.2 n. mi., 5 n. mi. to 135 n. mi.
Radio altimeter	Bendix	ALA-51	ALT	0 to 760 m		±0.6 m or 2 percent; -3 to 150 m ± 5 percent; 150 to 760 m
Inertial navigation system (INS)	Litton	LTN-51	Pitch	0 to 15°	0.04°	0.2°
			Roll	0 to 90°		
				15 to 30°	0.04°	0.5°
				30 to 90°	0.04°	1.0°
			Heading	0 to 360°	0.1°	0.4°
			AX	±2 g		0.05 percent (1σ)
			AY	±2 g		0.05 percent (1σ)
			AZ	±2 g (about 1 g)	0.001 g	0.01 g
			Latitude	0 to π rad	2.47 sec	
			Longitude	0 to π rad	2.47 sec	
			N/S velocity	±3276.7 knots	0.1 knot	
			E/W velocity	±3276.7 knots	0.1 knot	
			True heading	0 to 2π rad	2.64 min	
Central air data computer (CADS)	Sperry		Pressure altitude	-305 m to 15,240 m	0.005 in./HG	±4.6 m, -30 to SL; ±6.1 m at 3050 m; ±12.2 m at 9150 m; ±24.2 m at 15,250 m
			Pressure altitude rate	0 to +6100 m/min	3 m/min	±9.1 m/min or 5 percent
			Calibrated airspeed	50 to 450 knots	0.25 knot	±5 knots at 60 knots
			MACH	0.2 to 1.0 m		±2 knots at 100 knots; ±2 knots at 200 knots; ±0.015 m, 0.2 to 0.5 m; ±0.01 m, 0.5 to 0.95 m; ±0.015 m, 0.95 to 1.0 m
			True airspeed	150 to 599 knots	1 knot	±4 knots

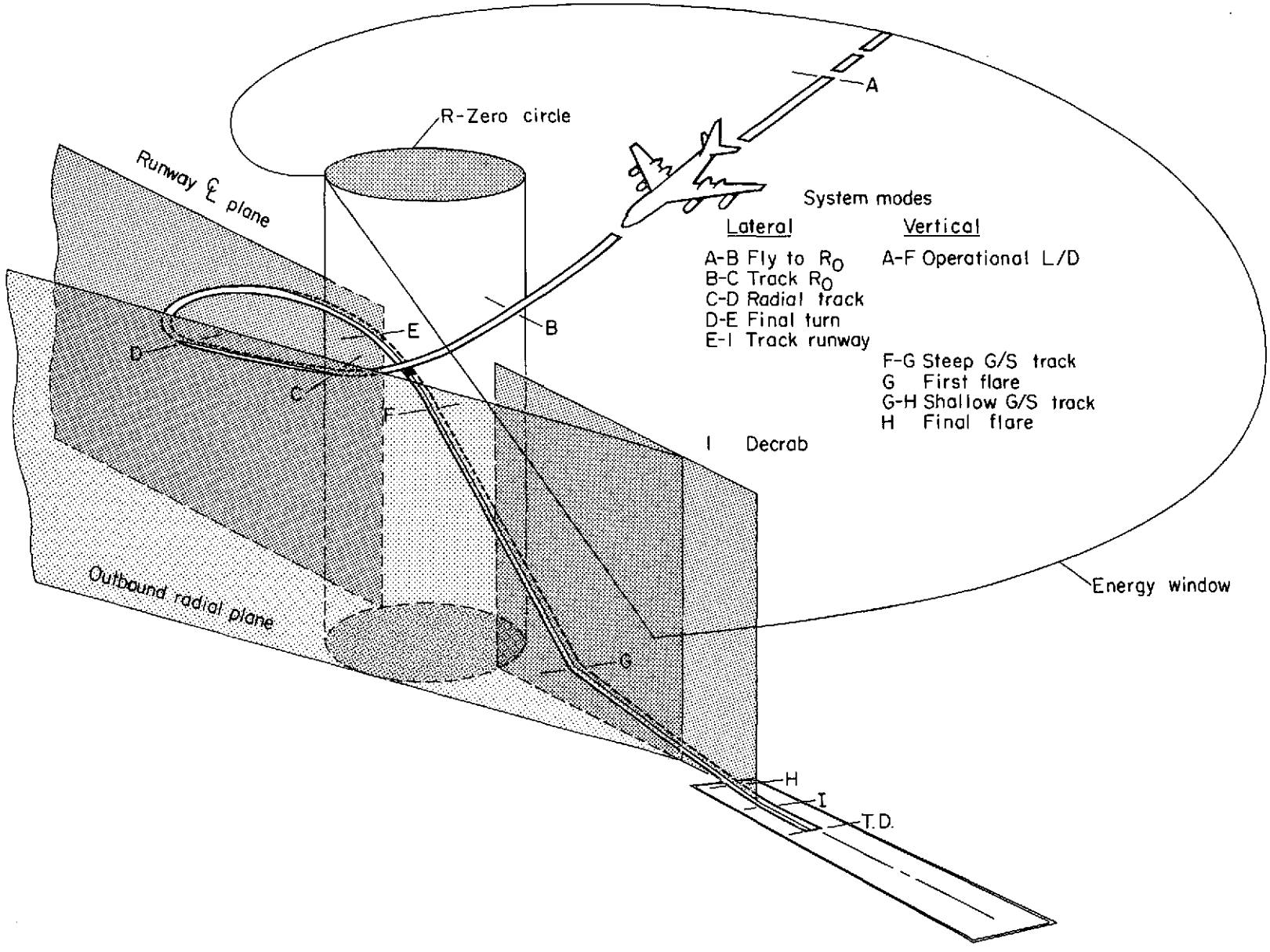

Figure 1.– Approach trajectory guidance concept.

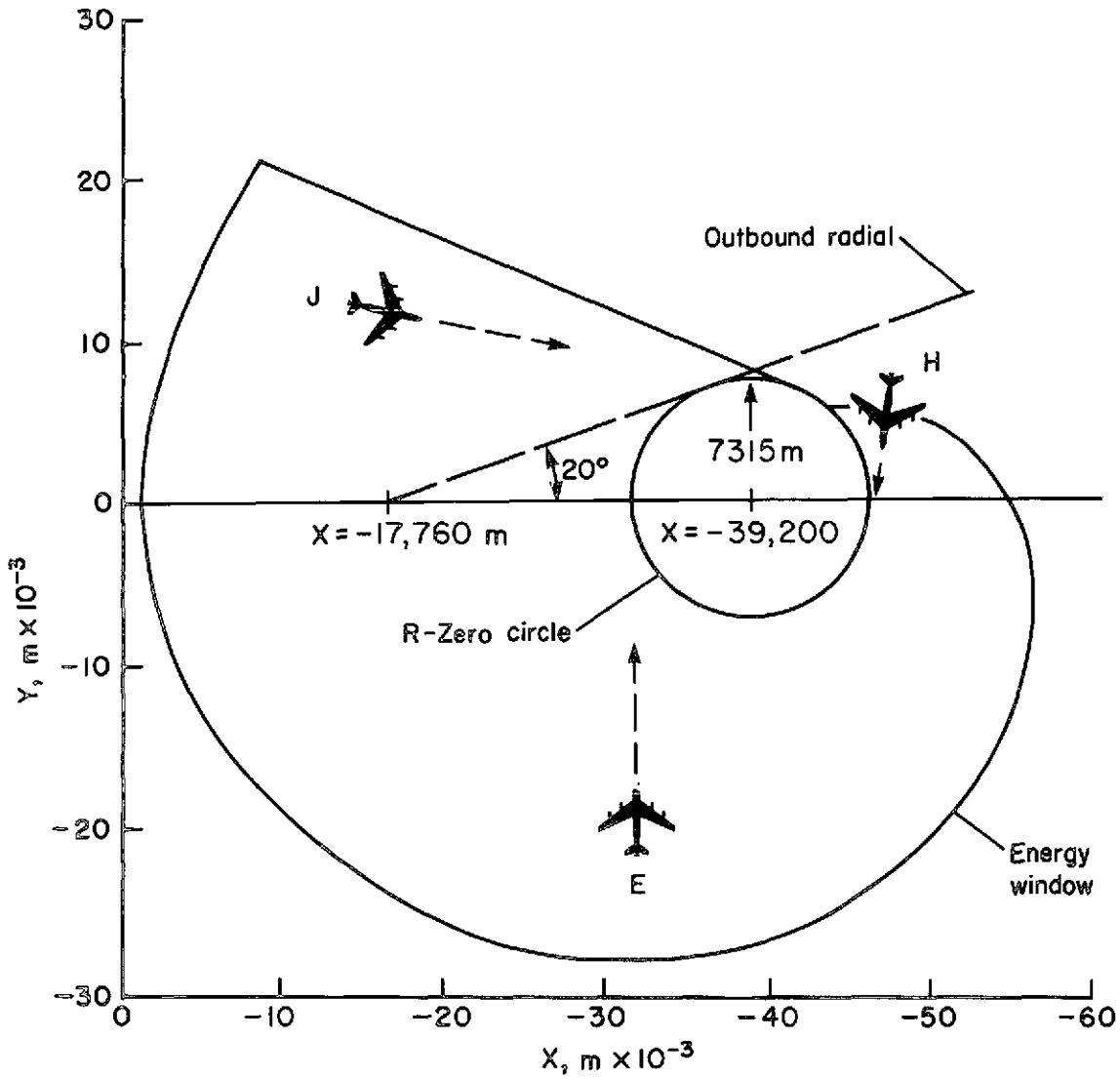

Figure 2.– CV-990 SS-FTS acceptable window of initial conditions at altitude of 11,300 m (37,000 ft).

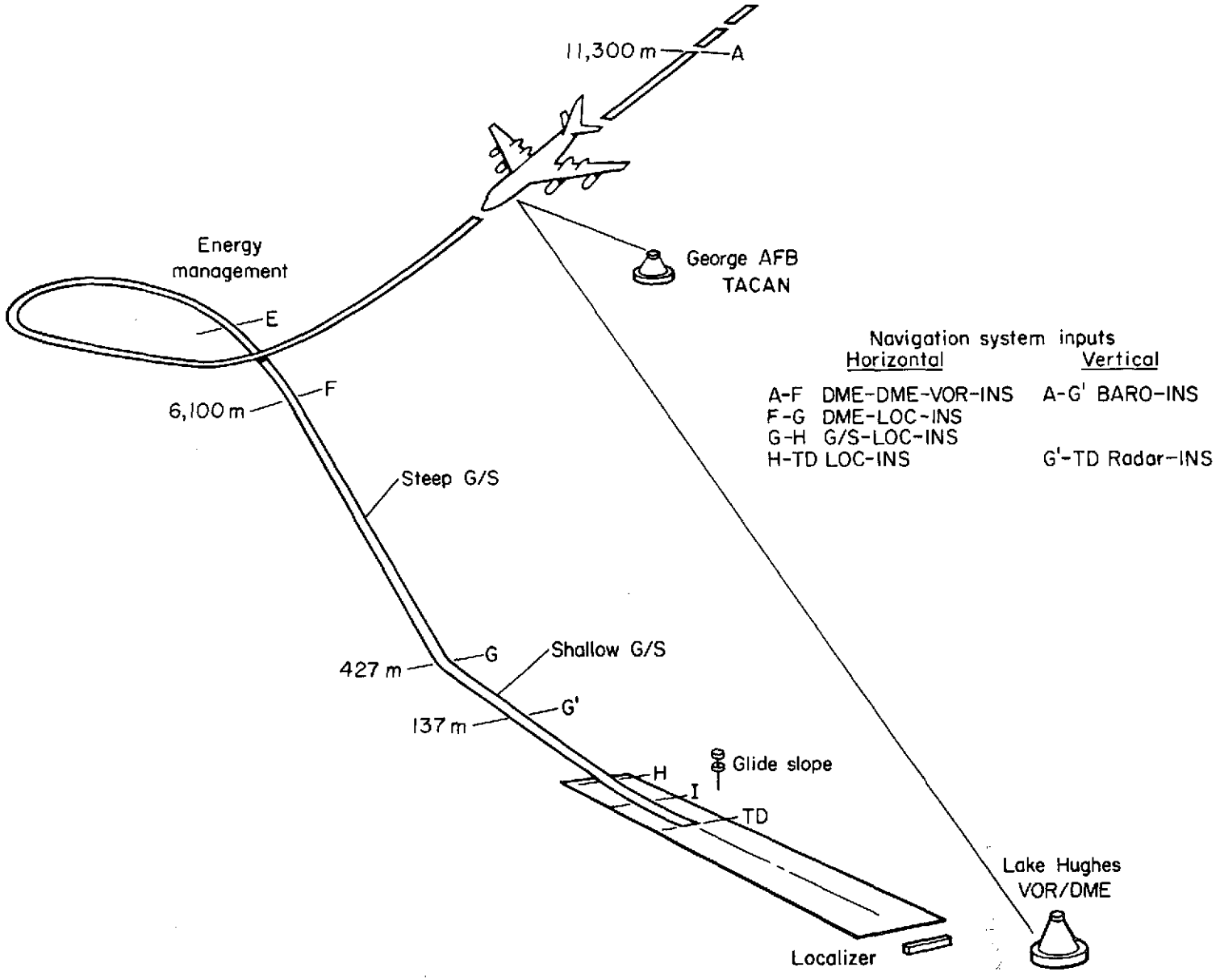

Figure 3.– Navigation concept.

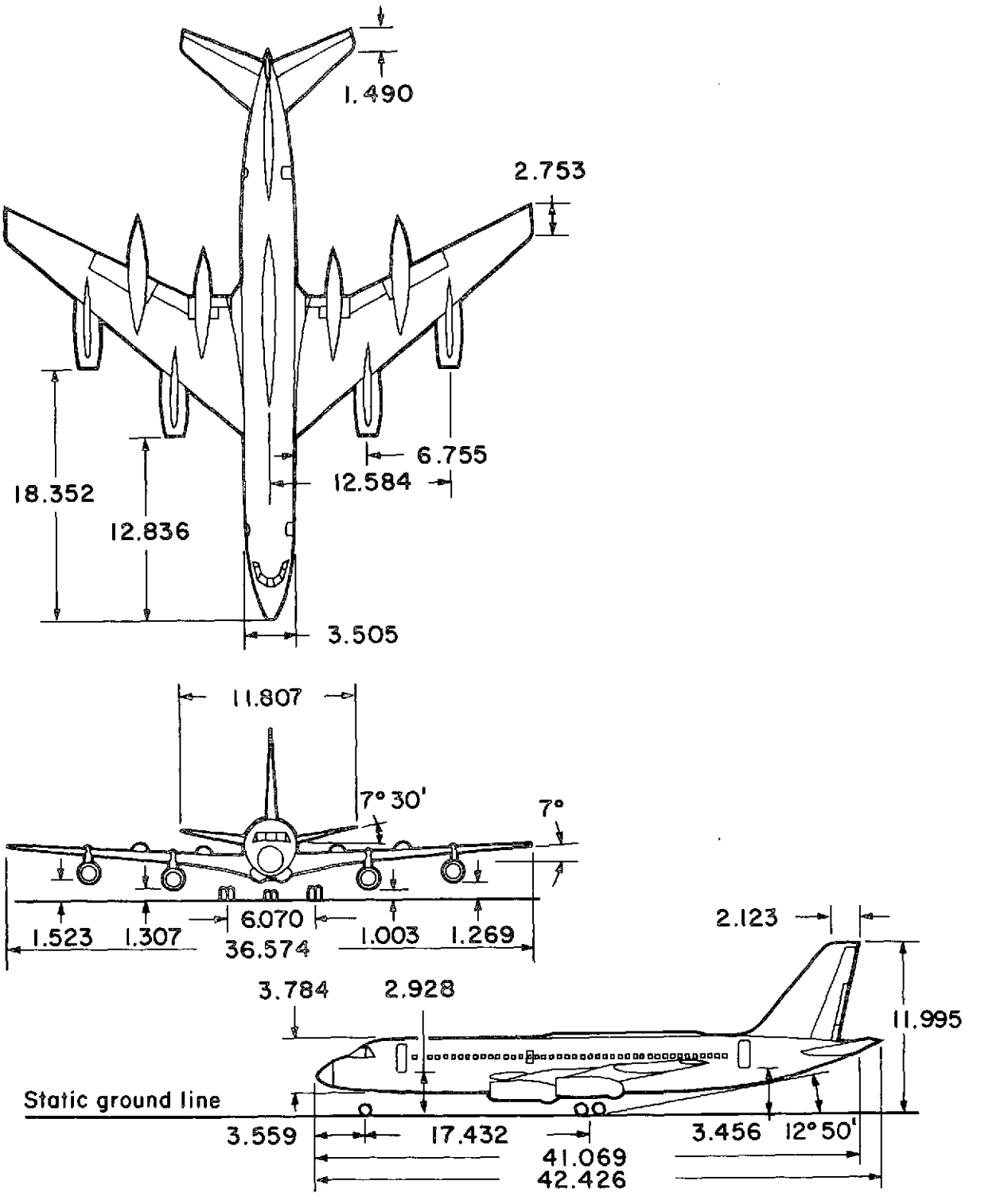

Figure 4.– General view and overall dimensions of the CV-990.

Figure 5.– CV-990 aircraft during simulated shuttle approach.

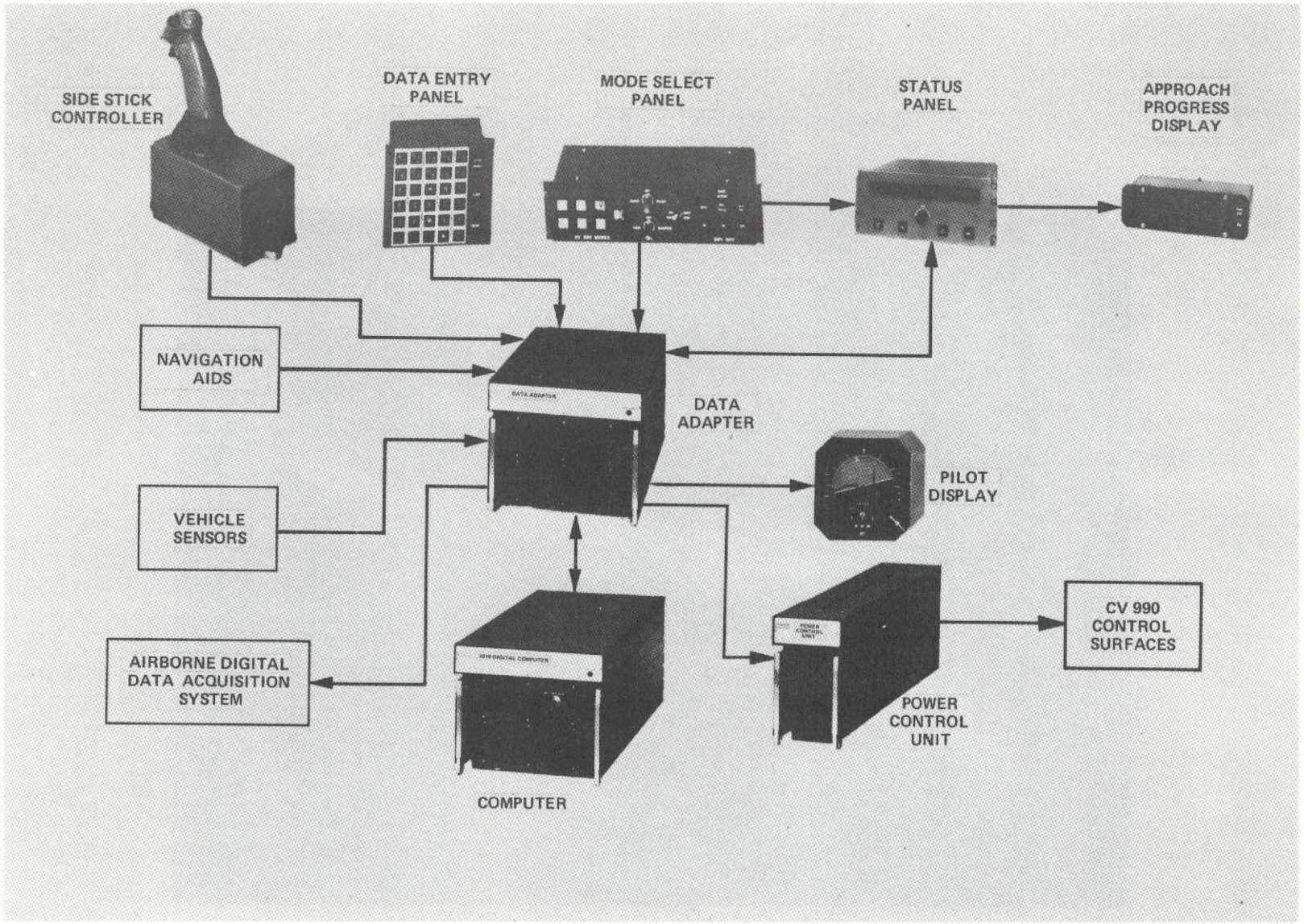

Figure 6.— Block diagram of the simulated shuttle flight test system.

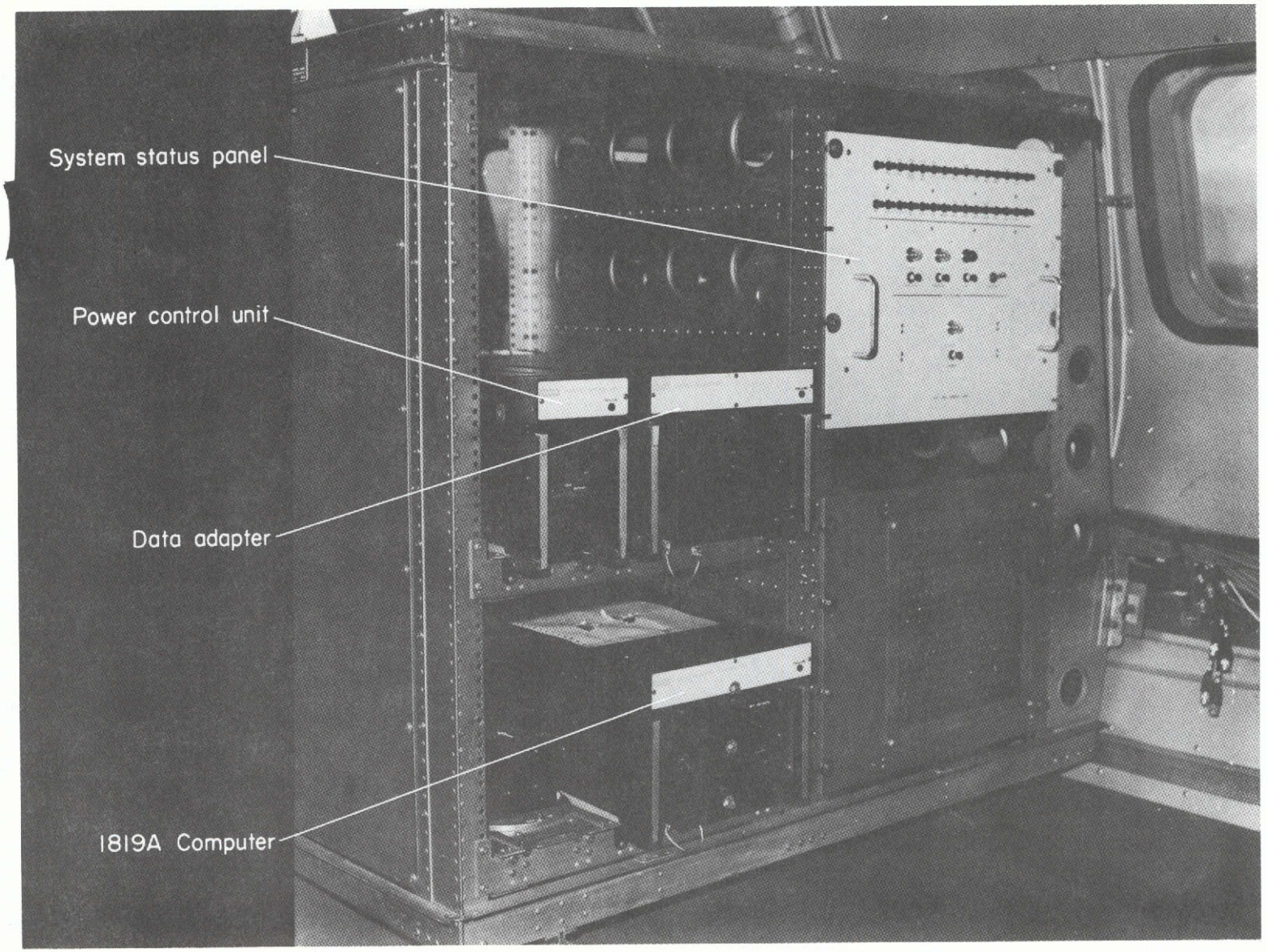

Figure 7.– Equipment rack.

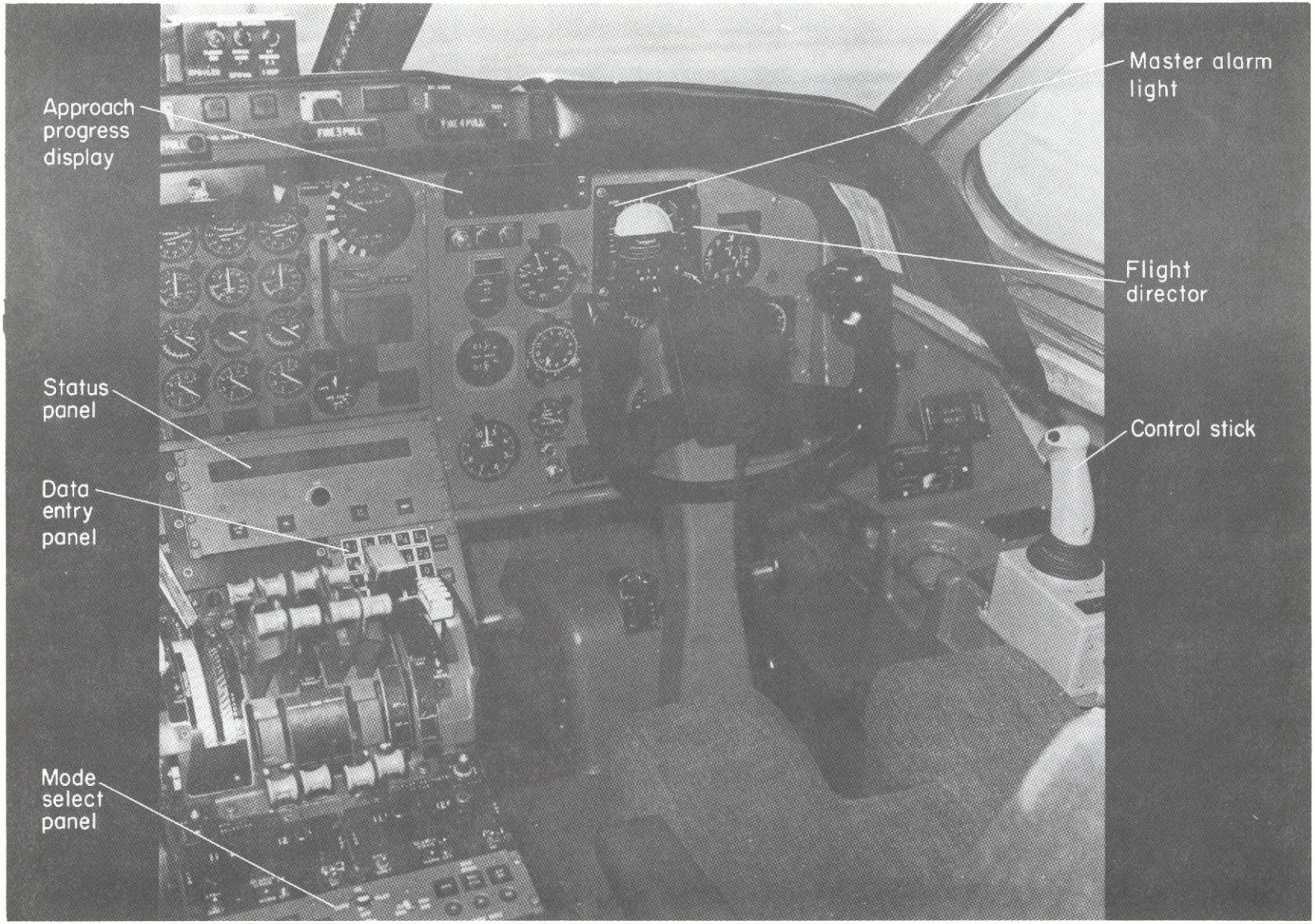

Figure 8.– CV-990 cockpit configured for shuttle simulation.

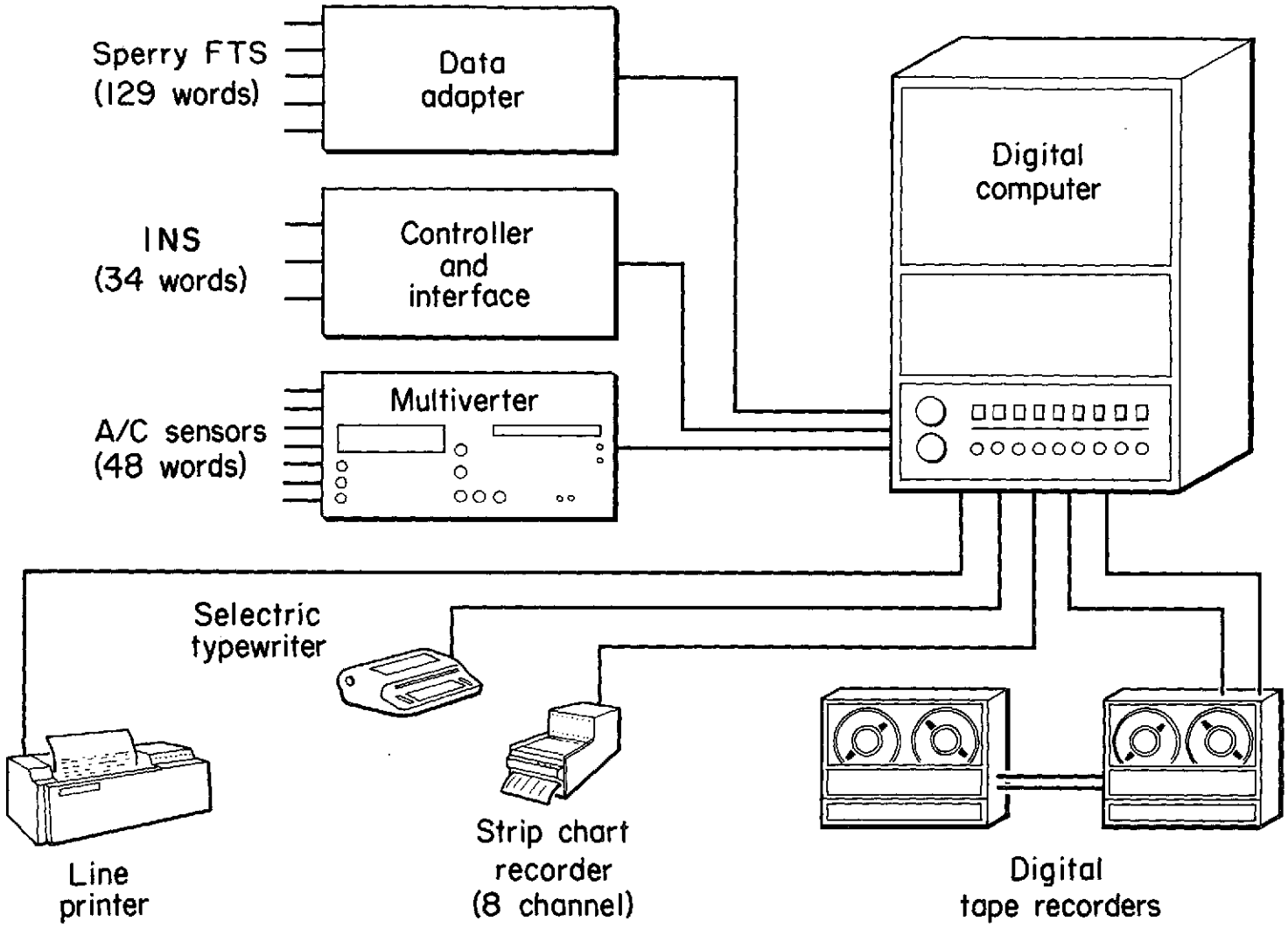

Figure 9.– Airborne digital data acquisition system (ADDAS).

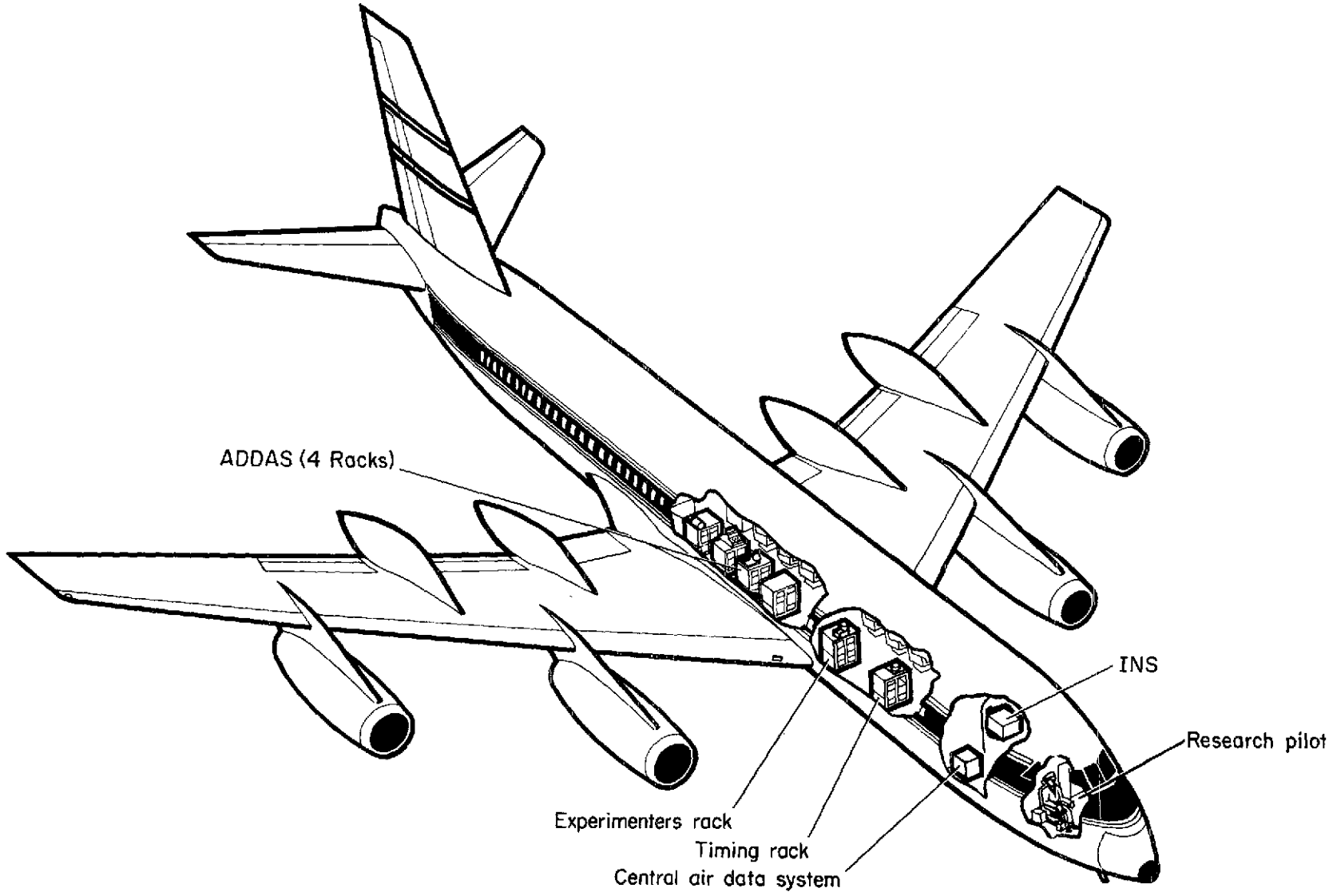

Figure 10.– Location of equipment in the CV-990.

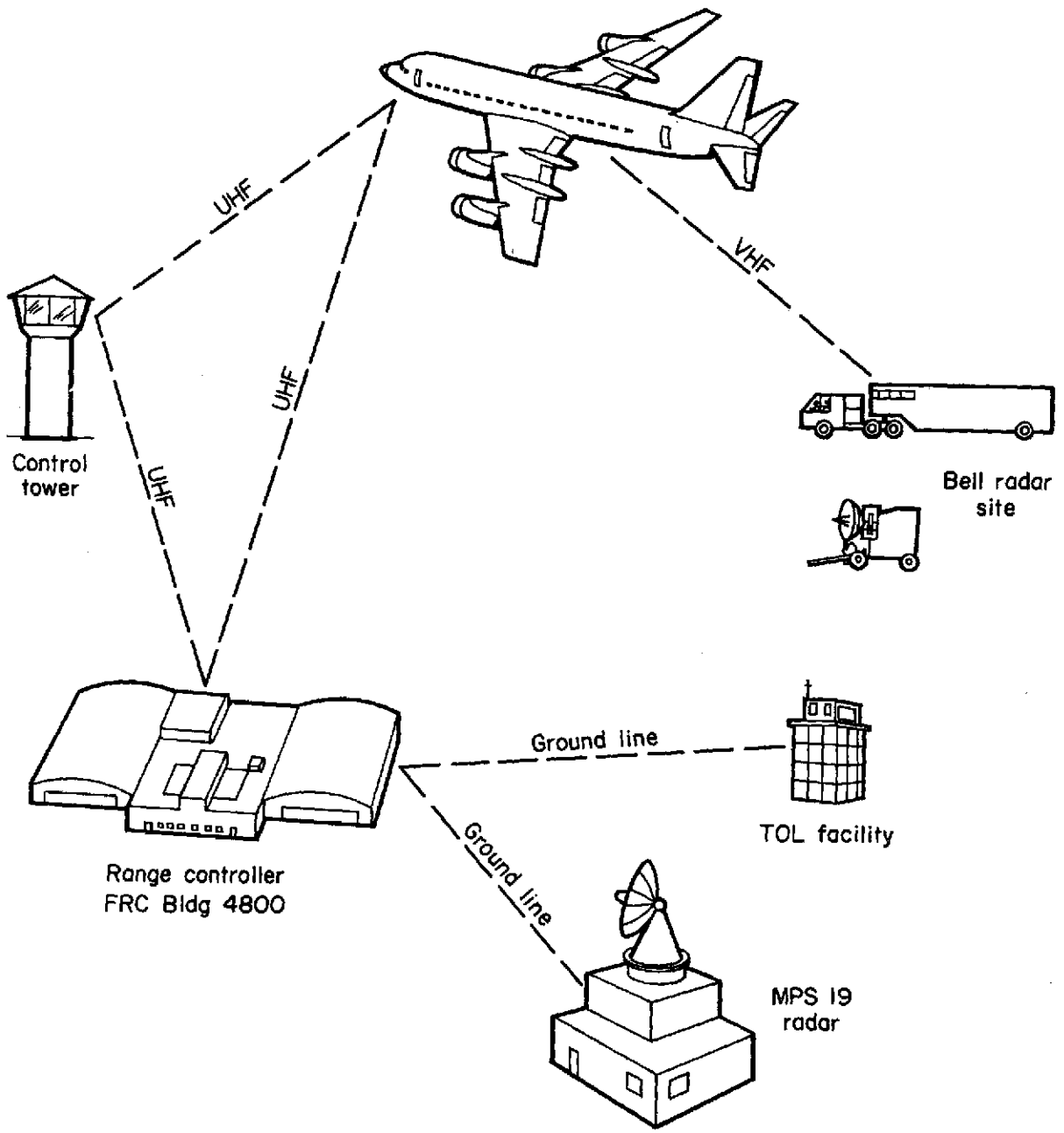

Figure 11.– Radio communication diagram.

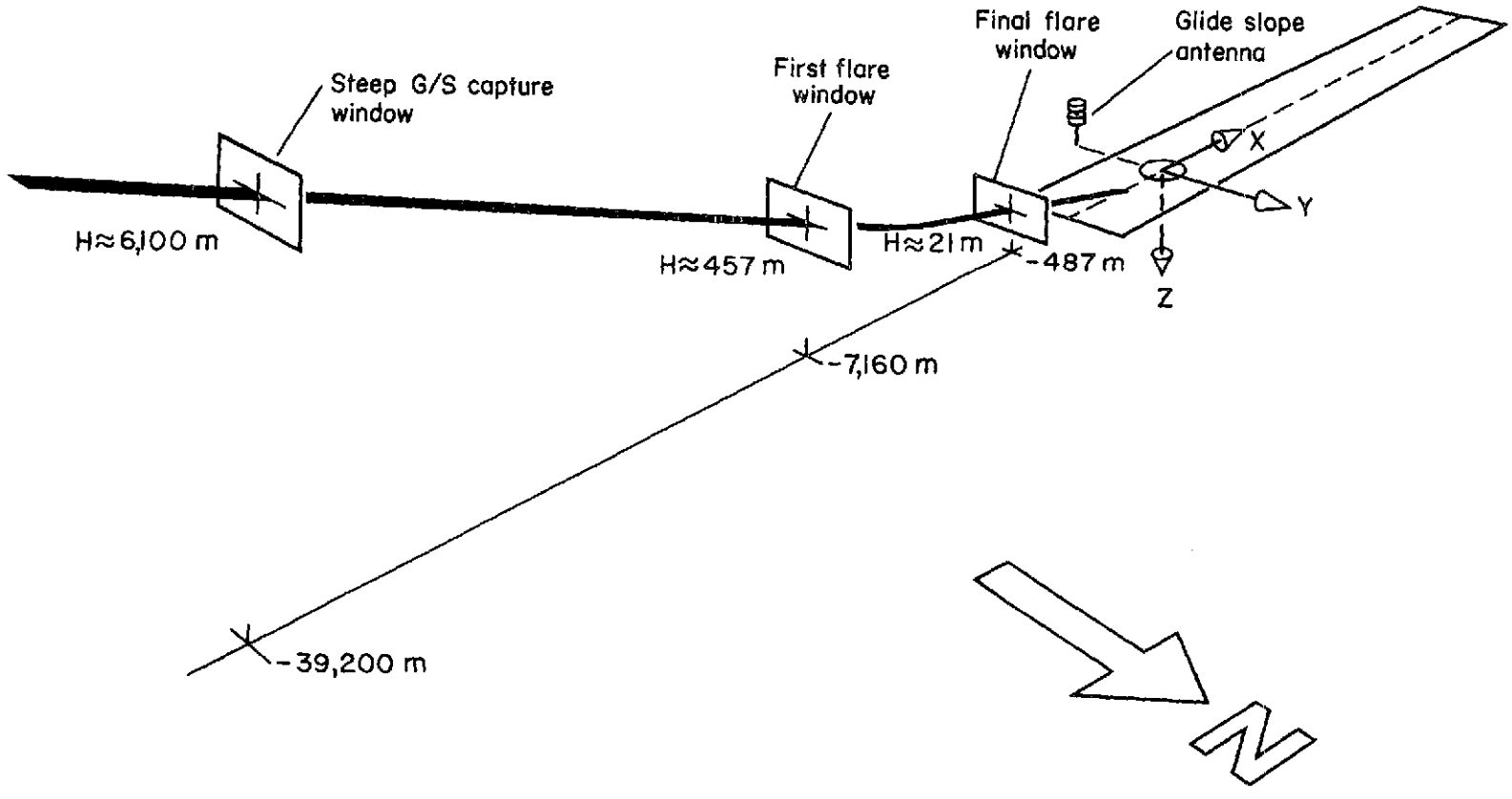

Figure 12.– Guidance and navigation window locations.

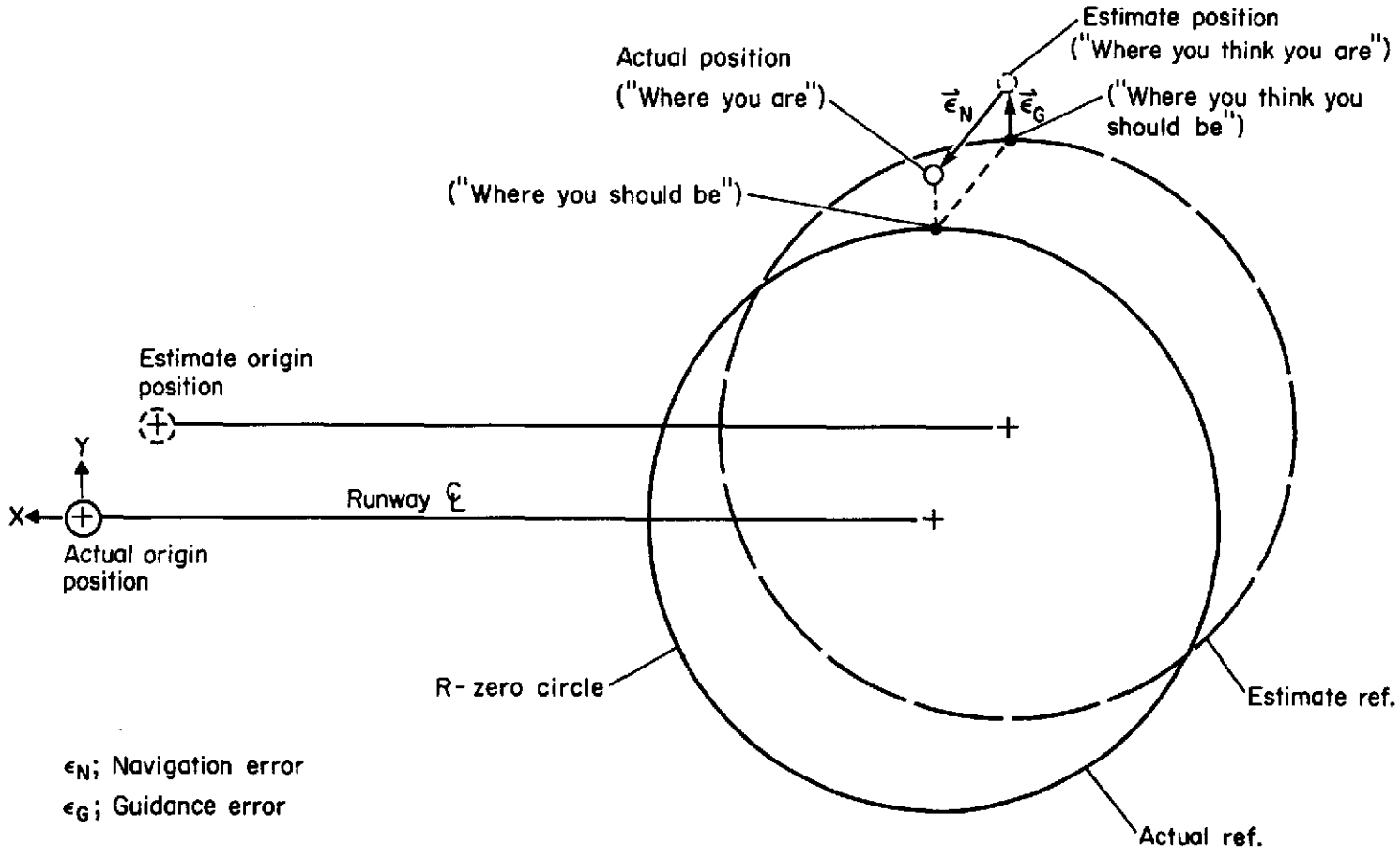

Figure 13.– Graphical description of navigation and guidance errors.

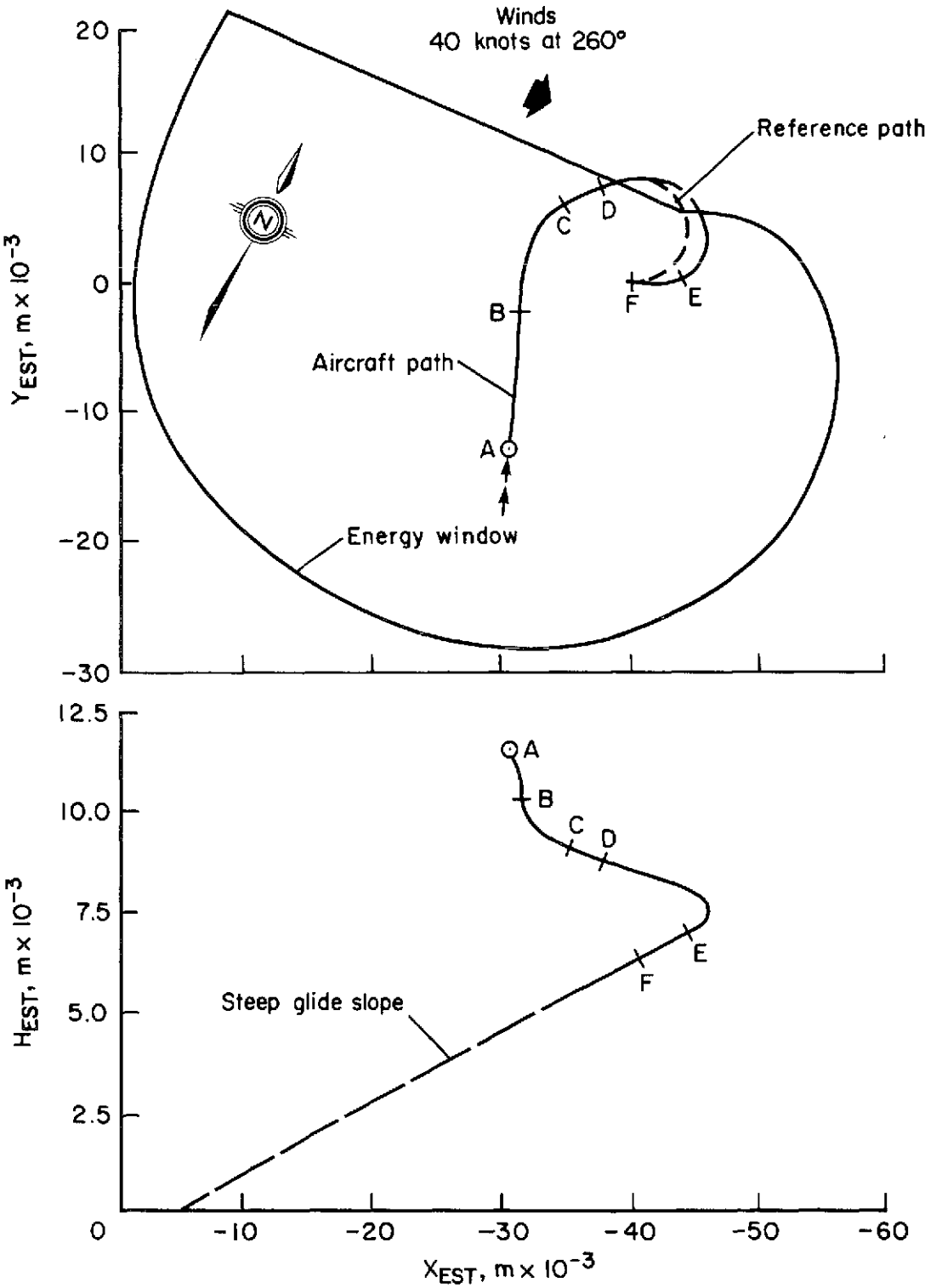

(a) Trajectory E.

Figure 14.– Energy management phase.

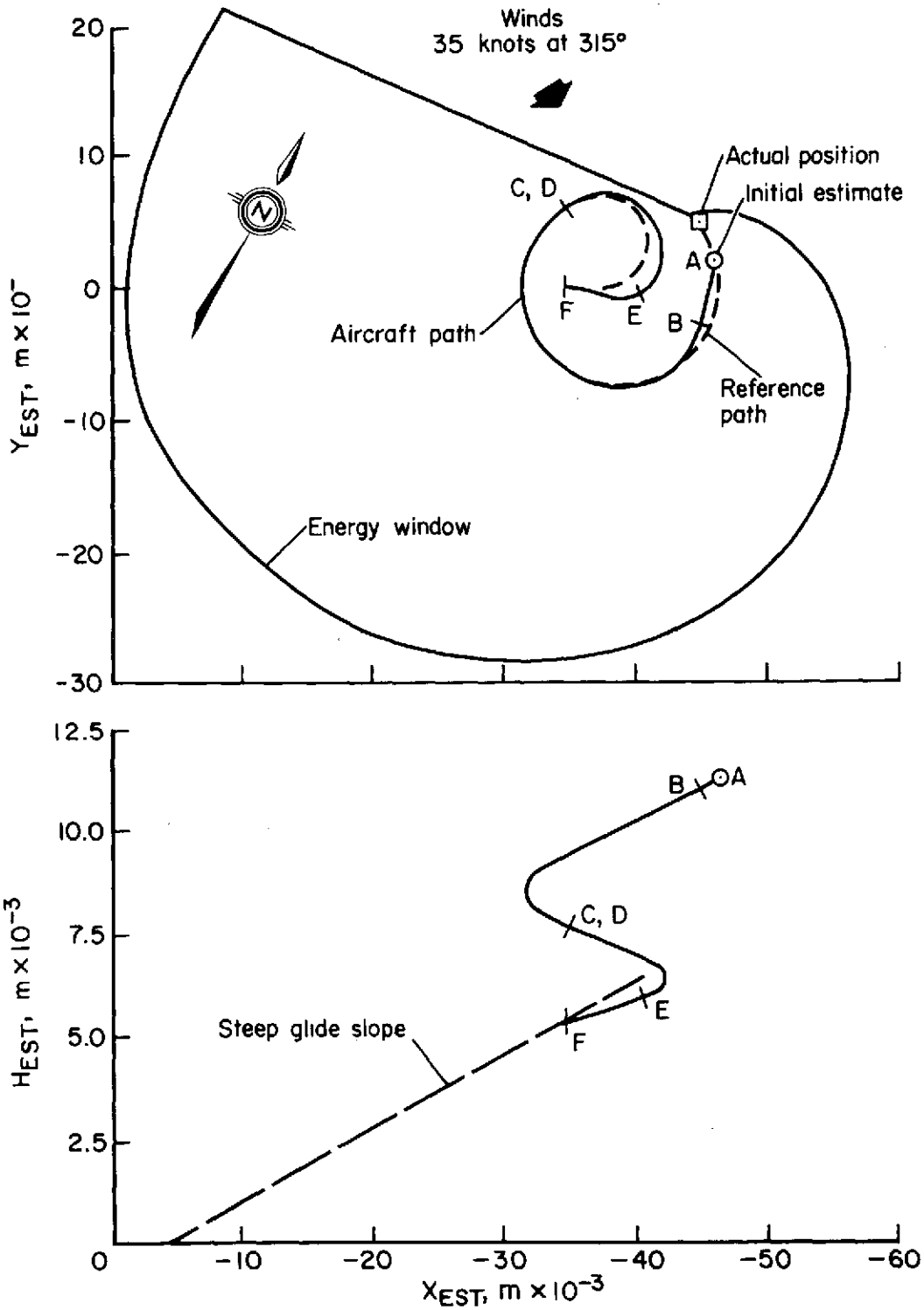

(b) Trajectory H.

Figure 14.– Concluded.

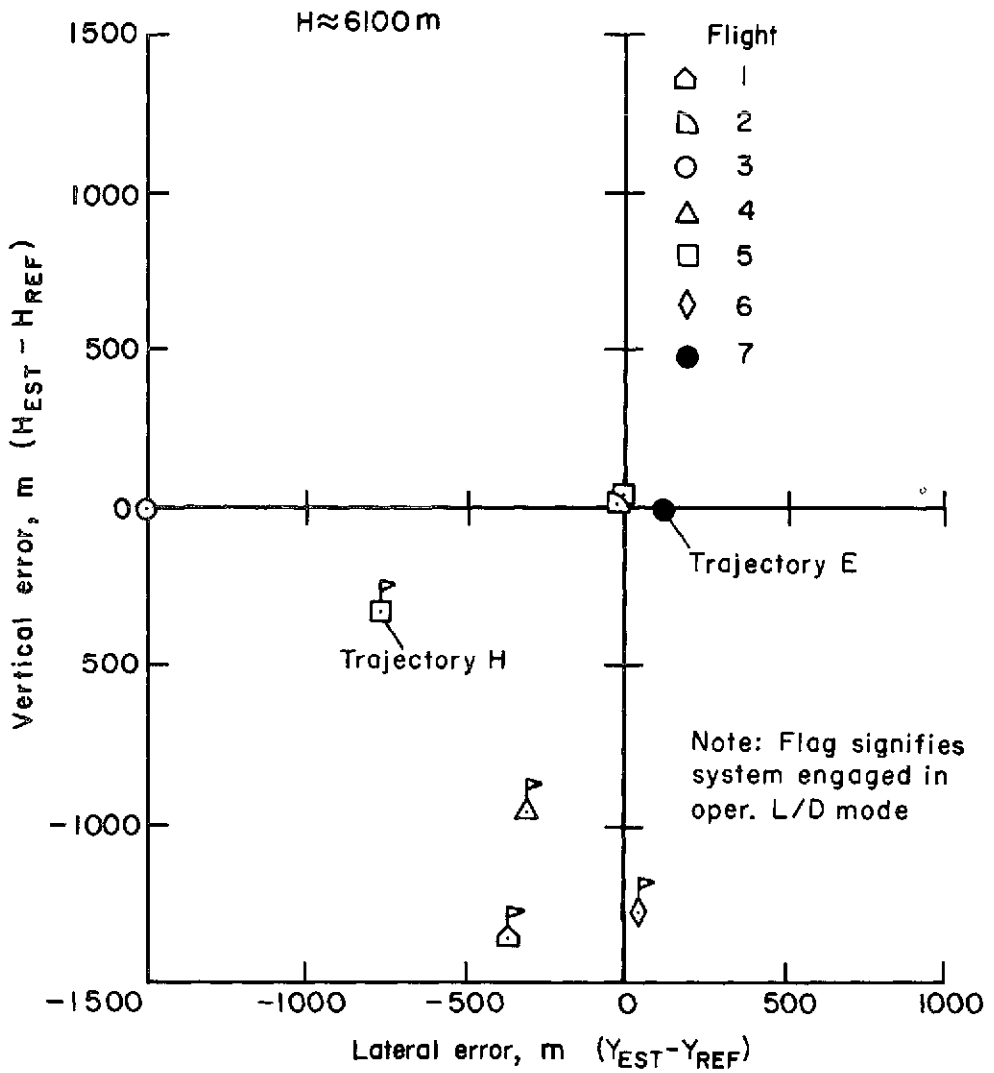

Figure 15.– Guidance error at steep glide-slope-capture window.

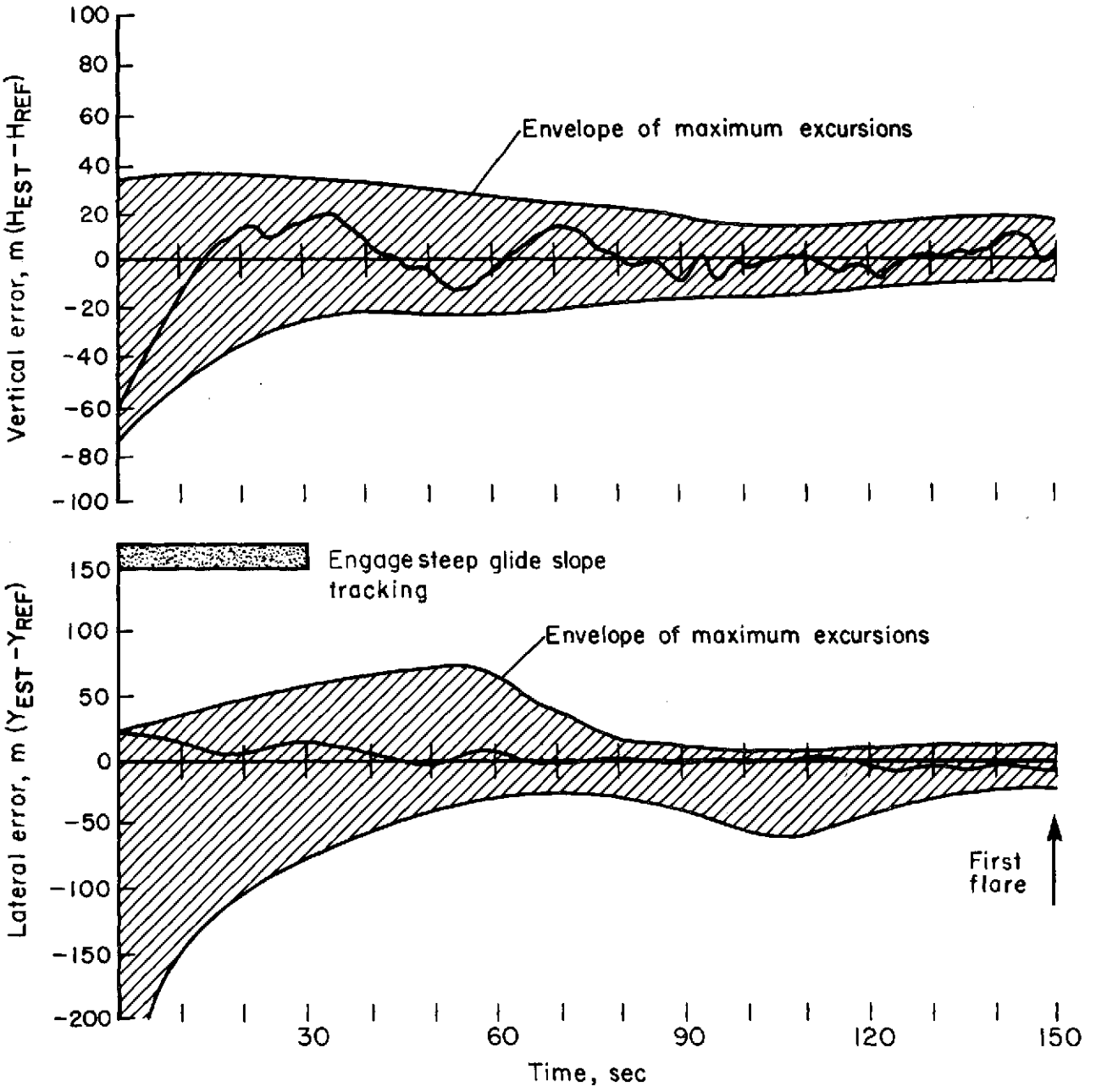

Figure 16.– Steep glide-slope tracking.

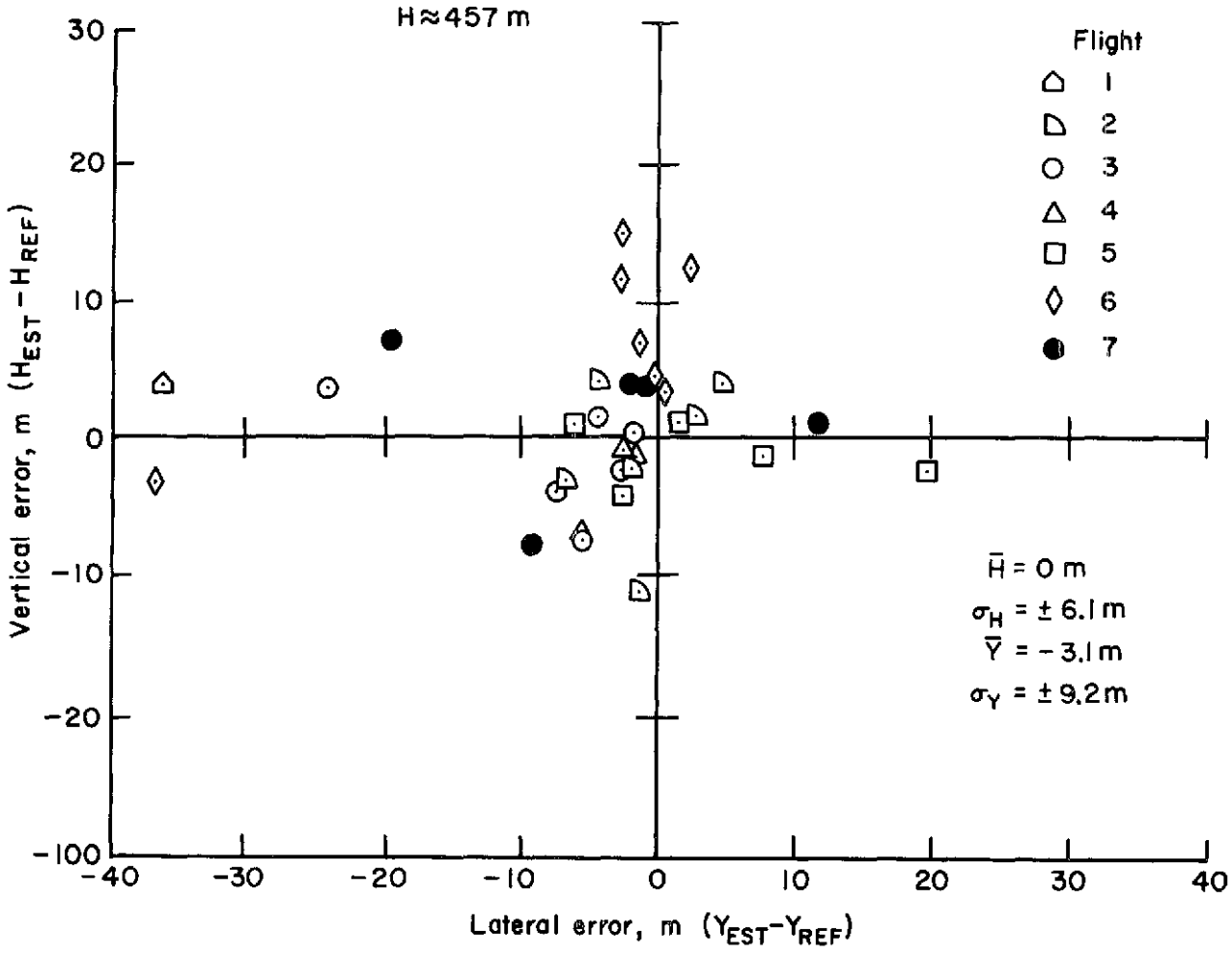

Figure 17.– Guidance error at first flare window.

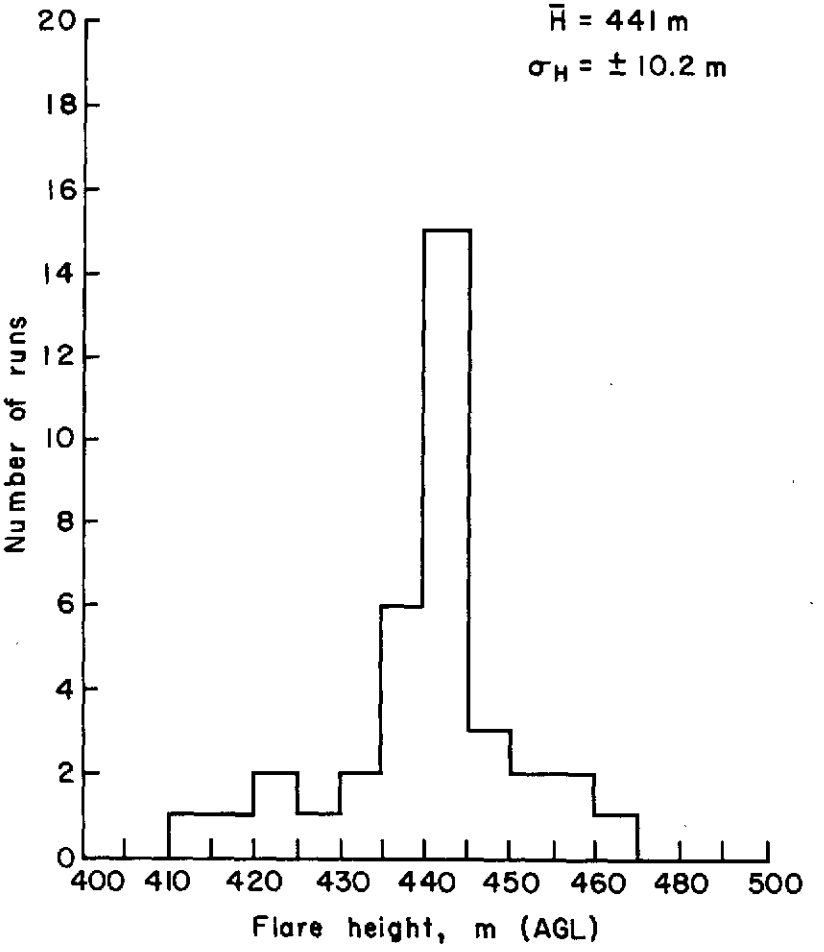

Figure 18.– Altitude of first flare.

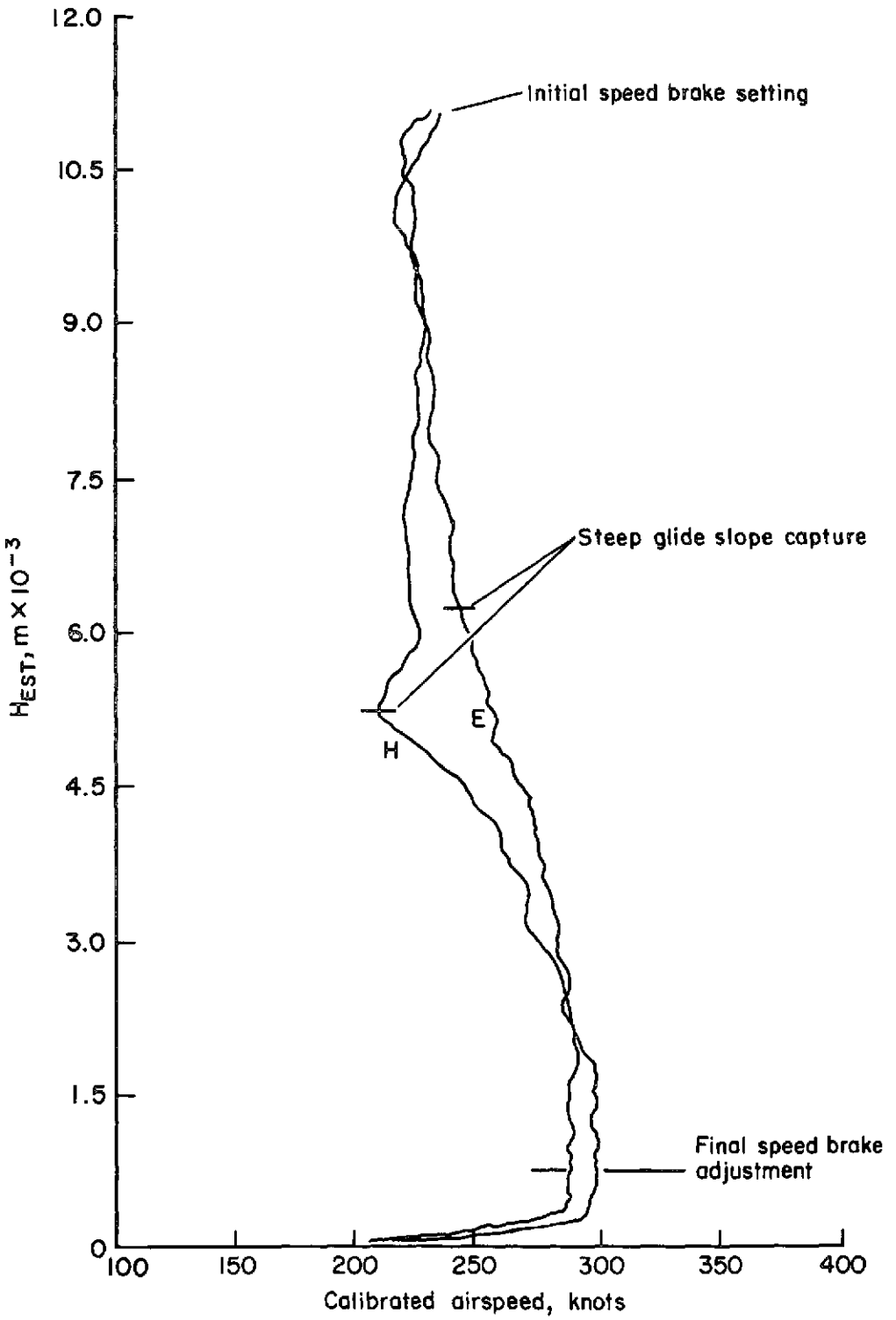

Figure 19.– Speed control during approach.

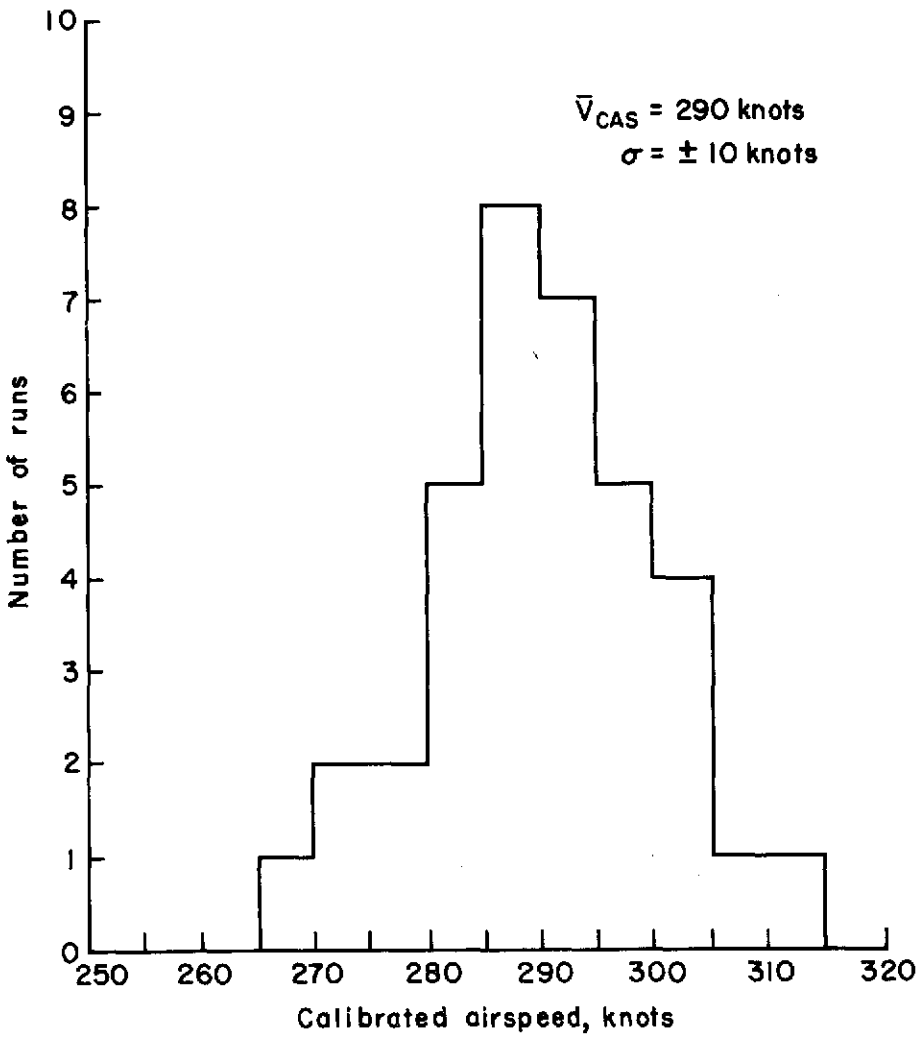

Figure 20.– Airspeed dispersions at nominal first flare altitude.

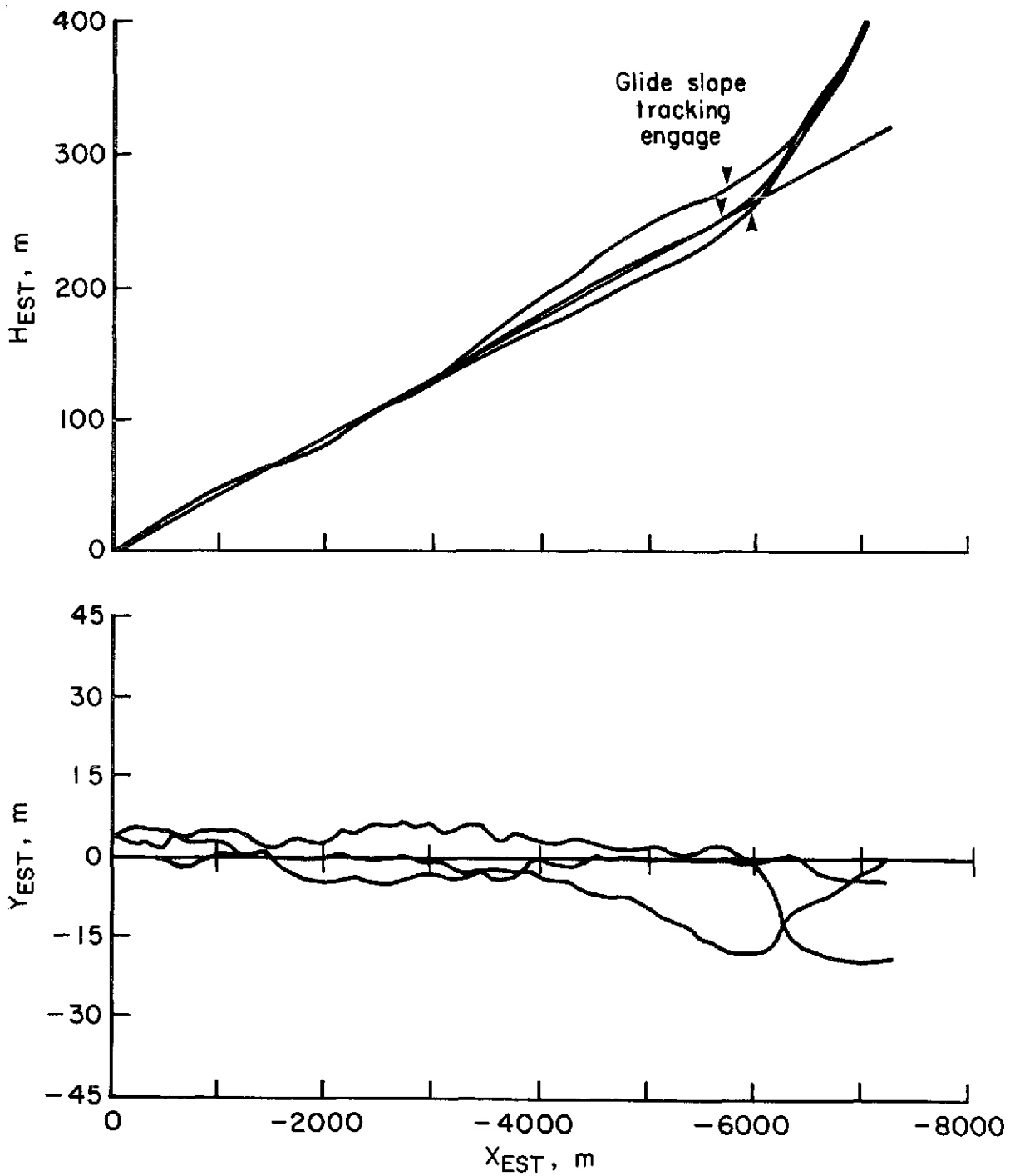

Figure 21.– First flare and shallow glide-slope tracking performance.

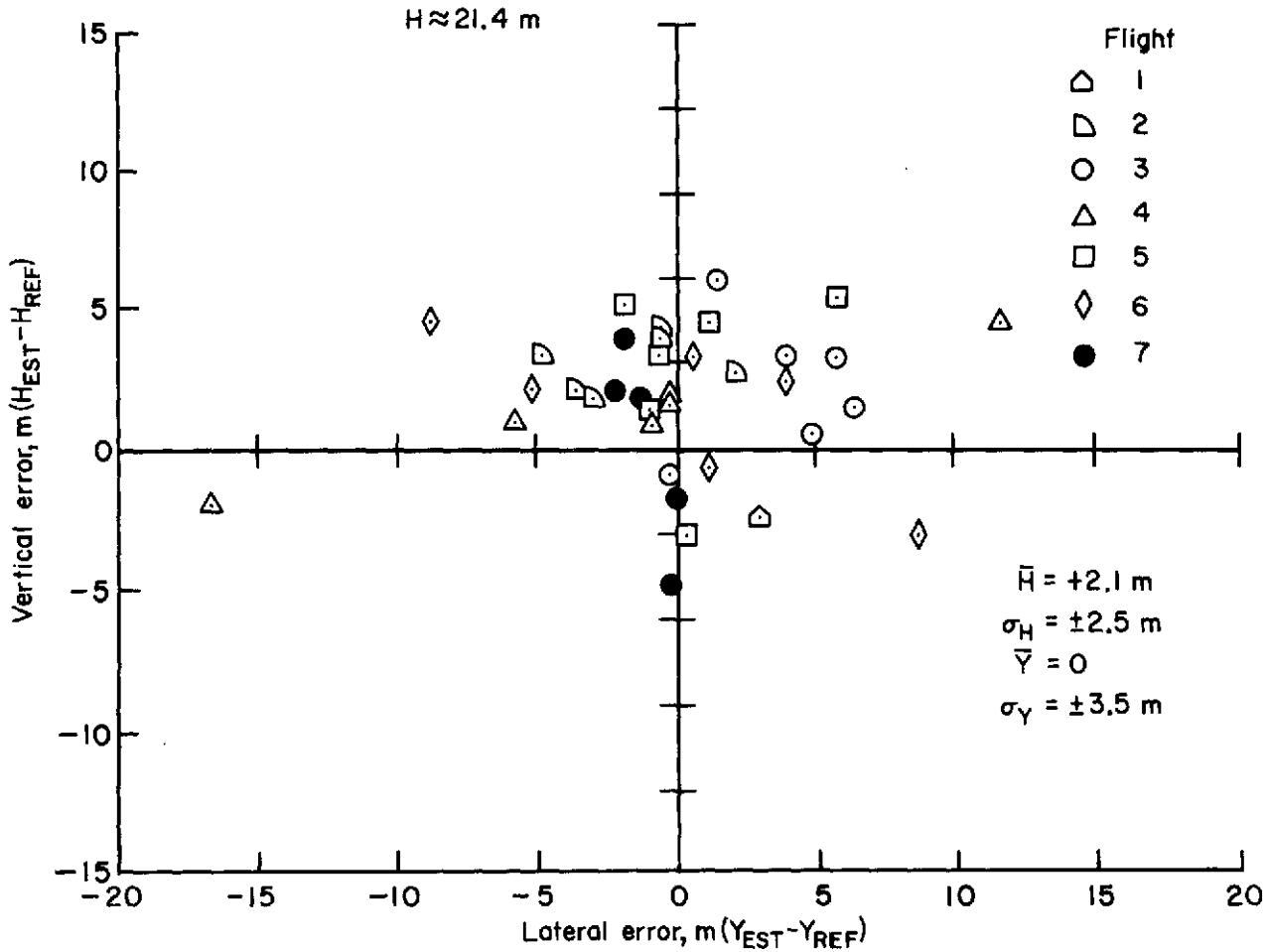

Figure 22.– Guidance error at final flare window.

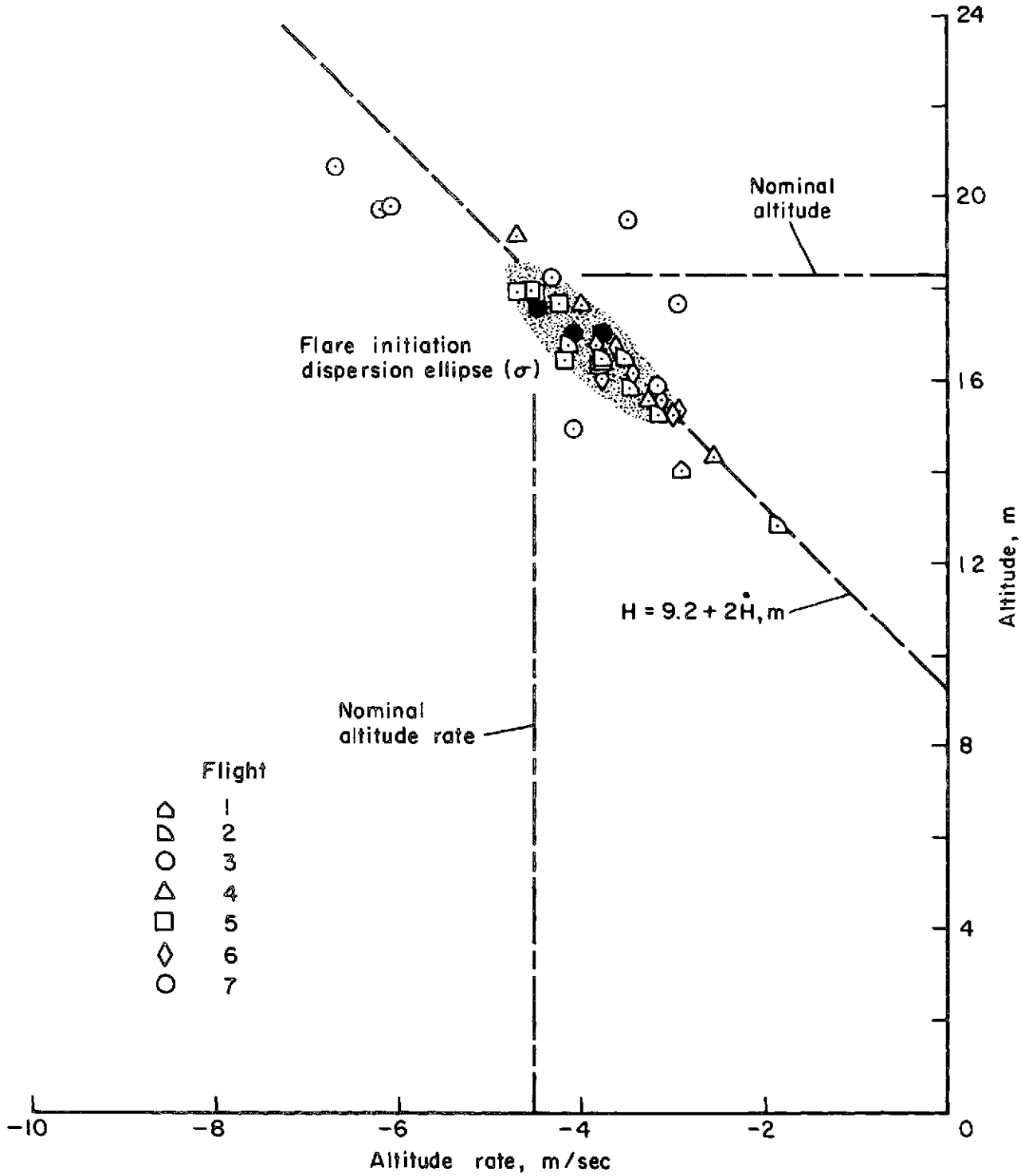

Figure 23.– Dispersions at final flare initiation.

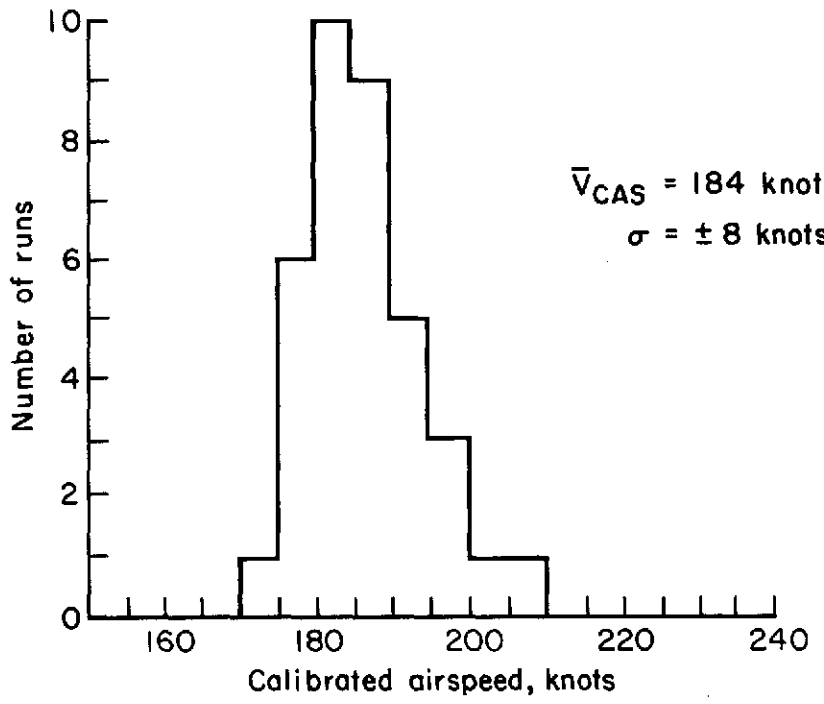

(a) Calibrated airspeed

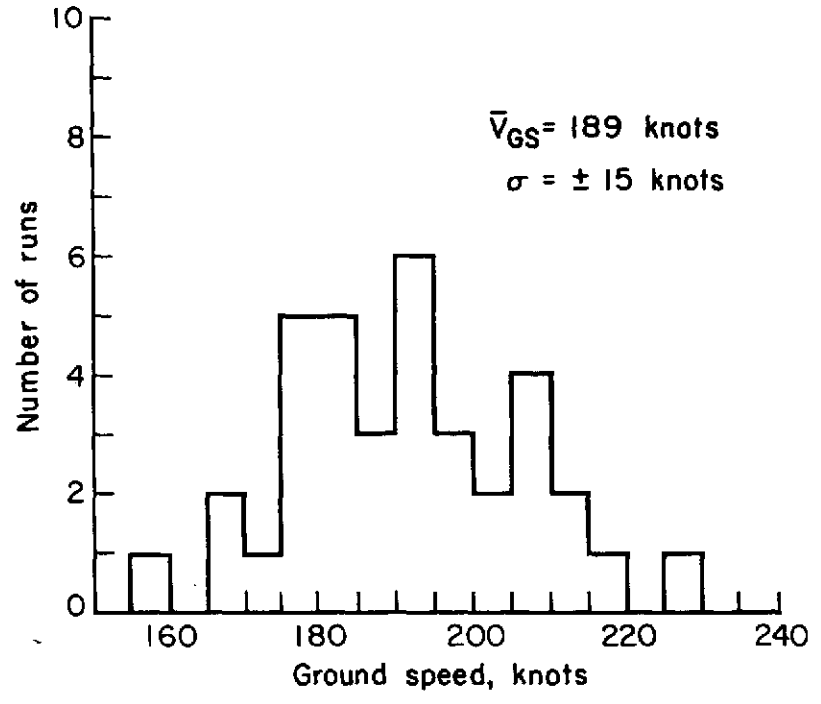

(b) Ground speed

Figure 24.– Speed dispersions at final flare.

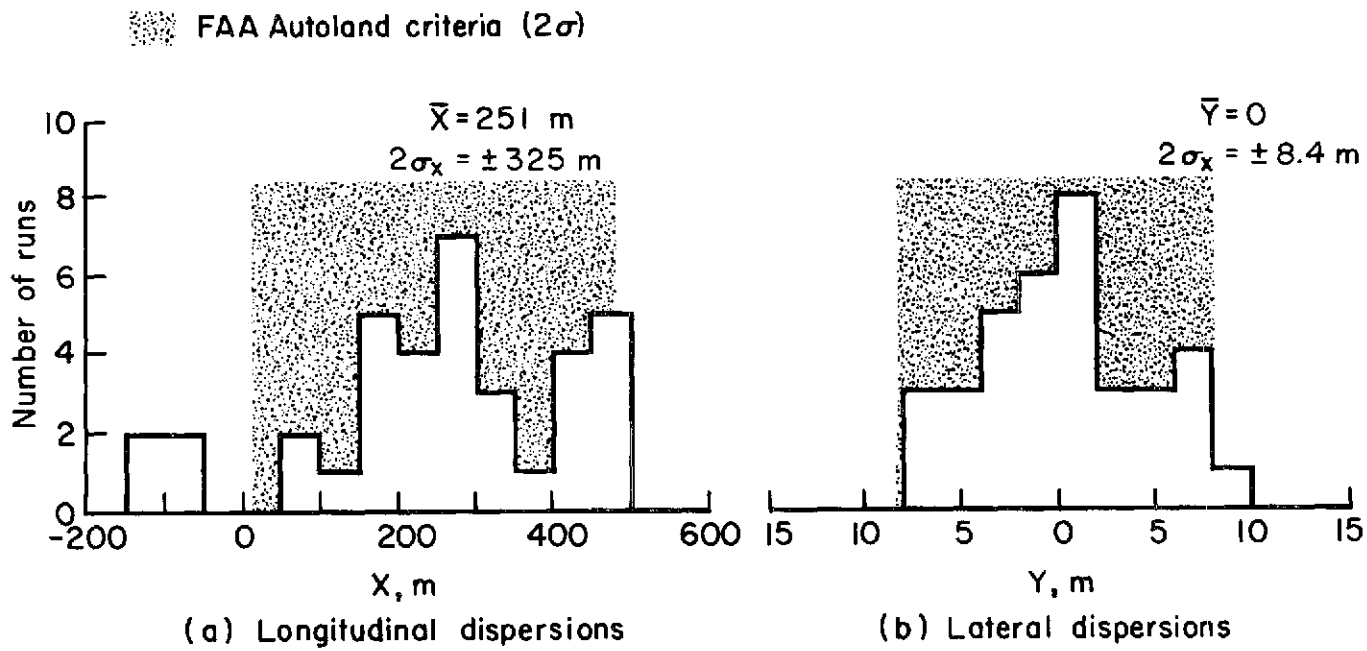

Figure 25.– Position dispersions at touchdown (TOL data).

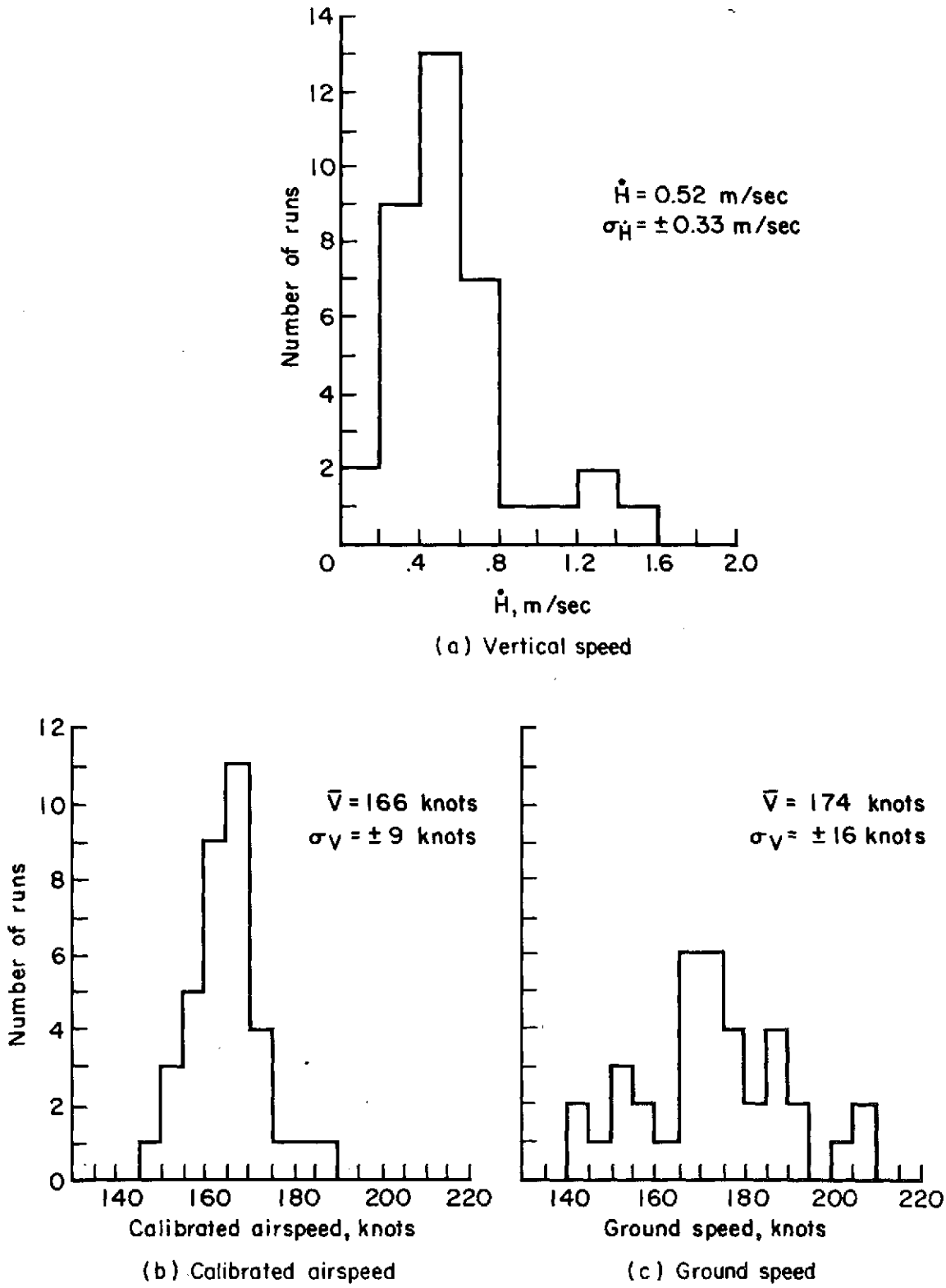

Figure 26.– Speed dispersions at touchdown.

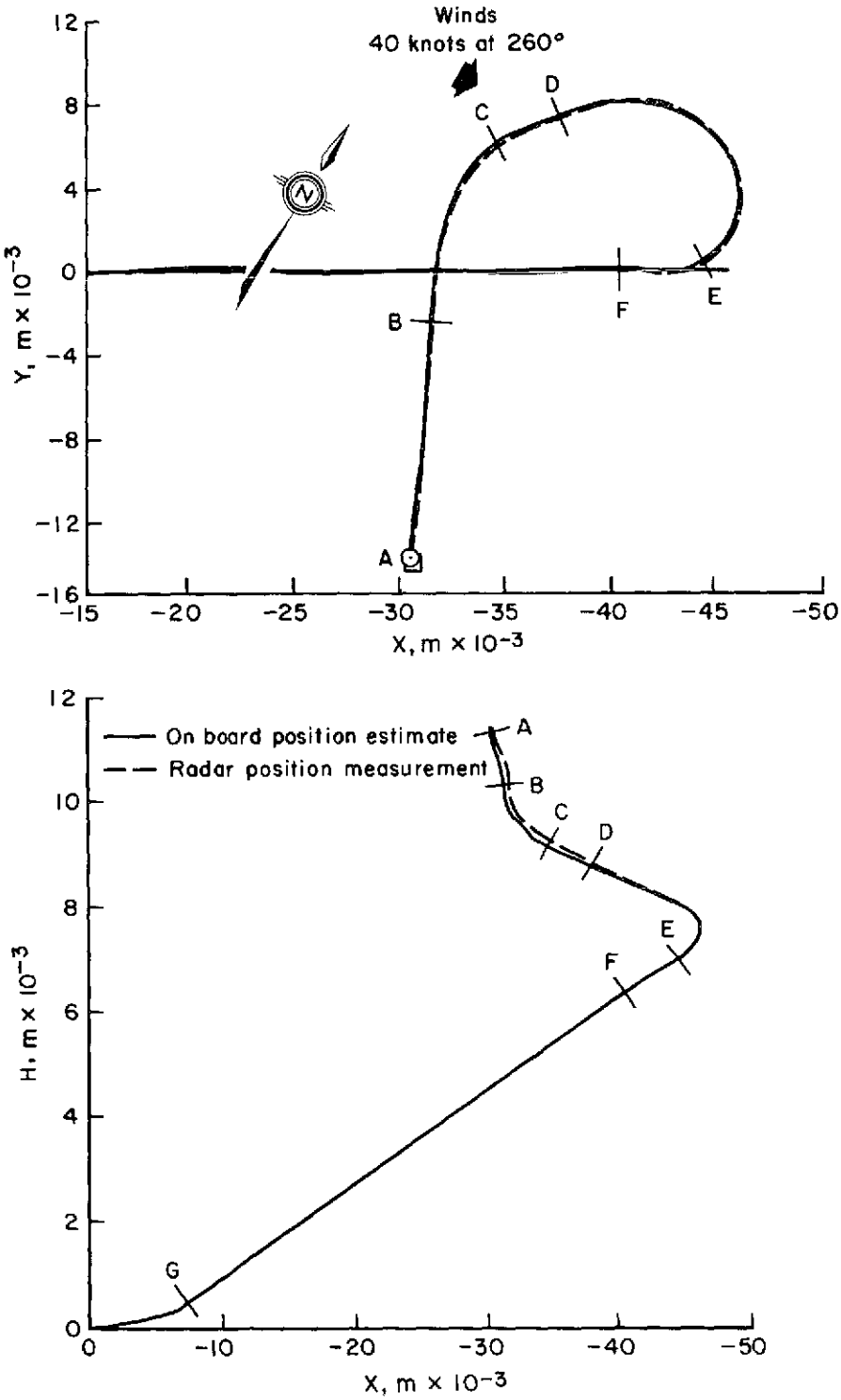

(a) Trajectory plot.

Figure 27.– Navigation performance during approach.

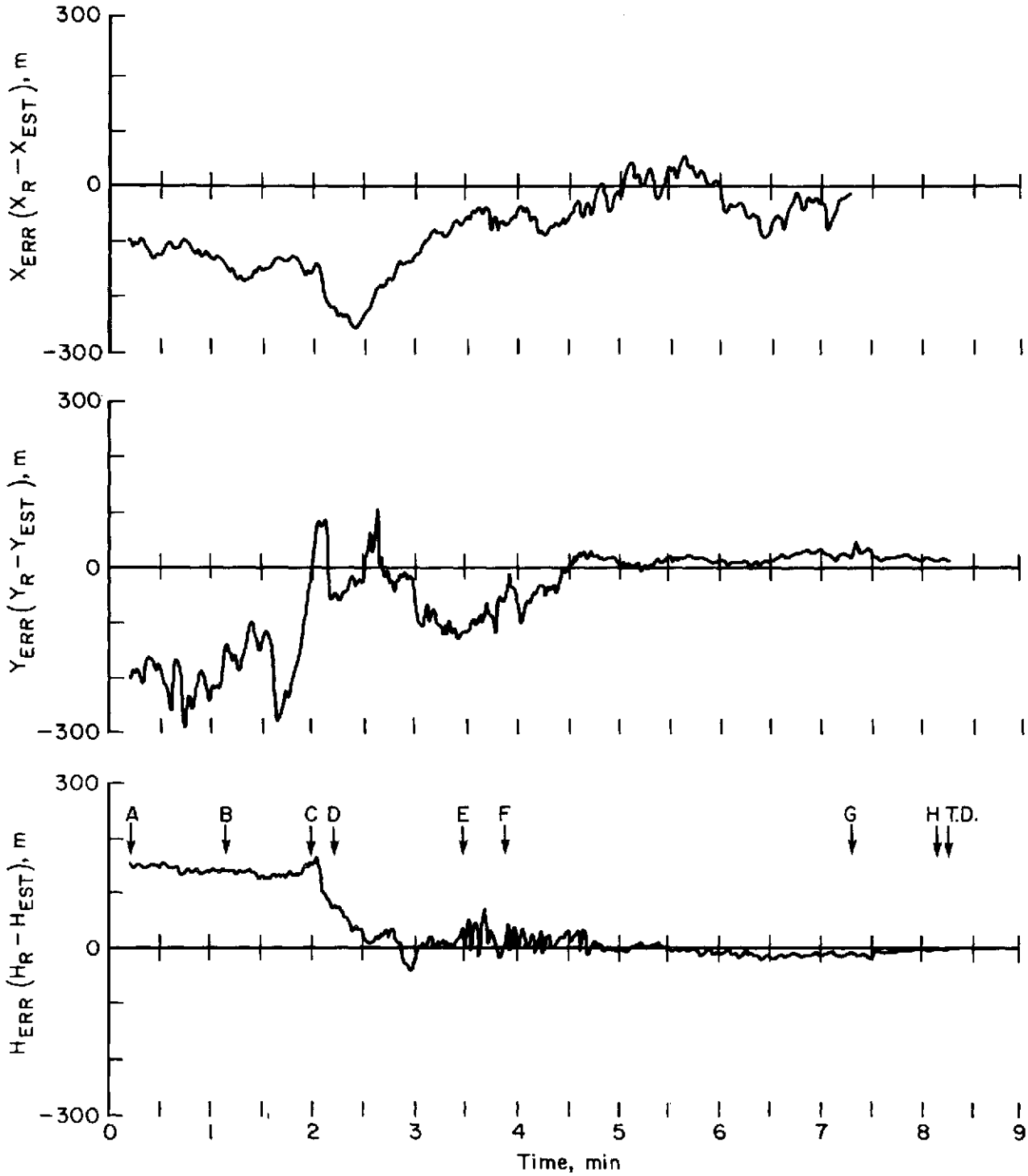

(b) Time histories of navigation errors.

Figure 27.— Concluded.

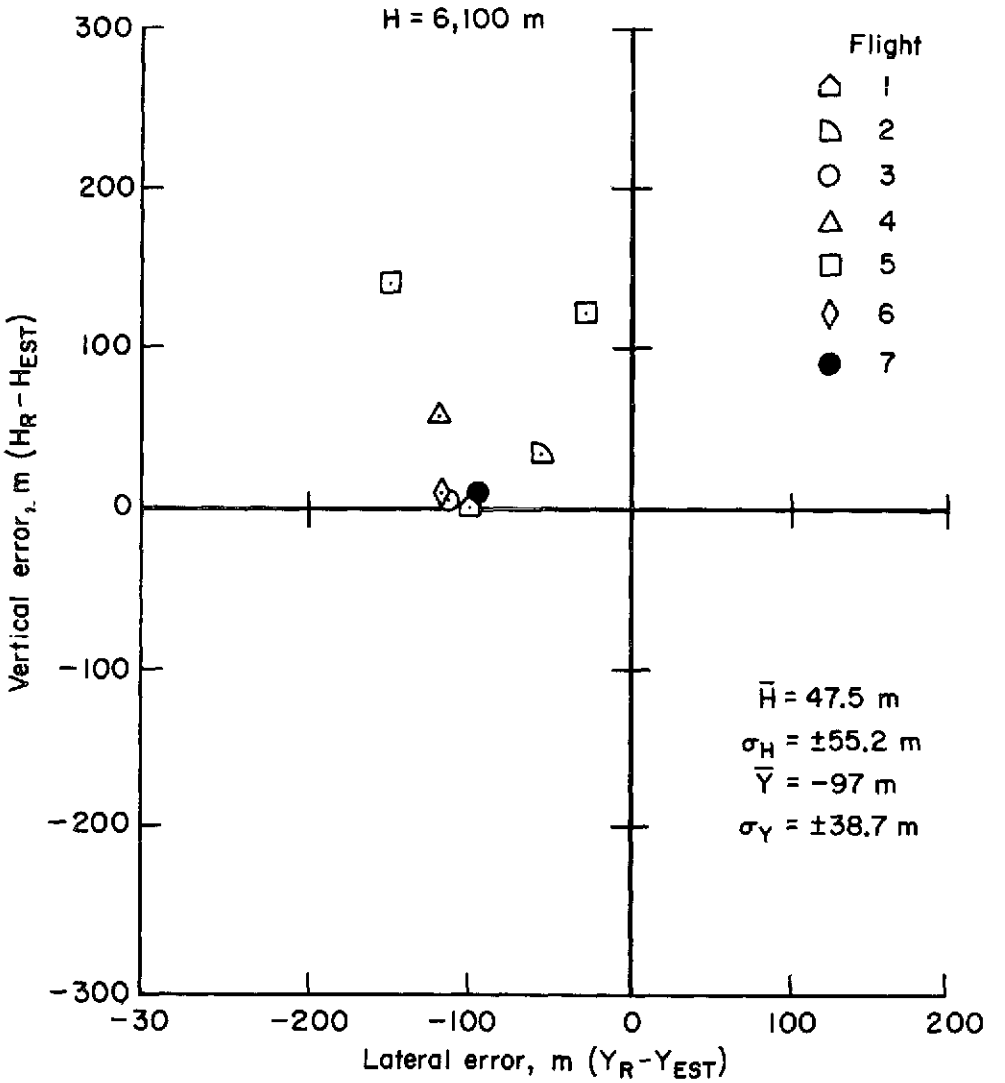

Figure 28.– Navigation errors at steep glide-slope capture window.

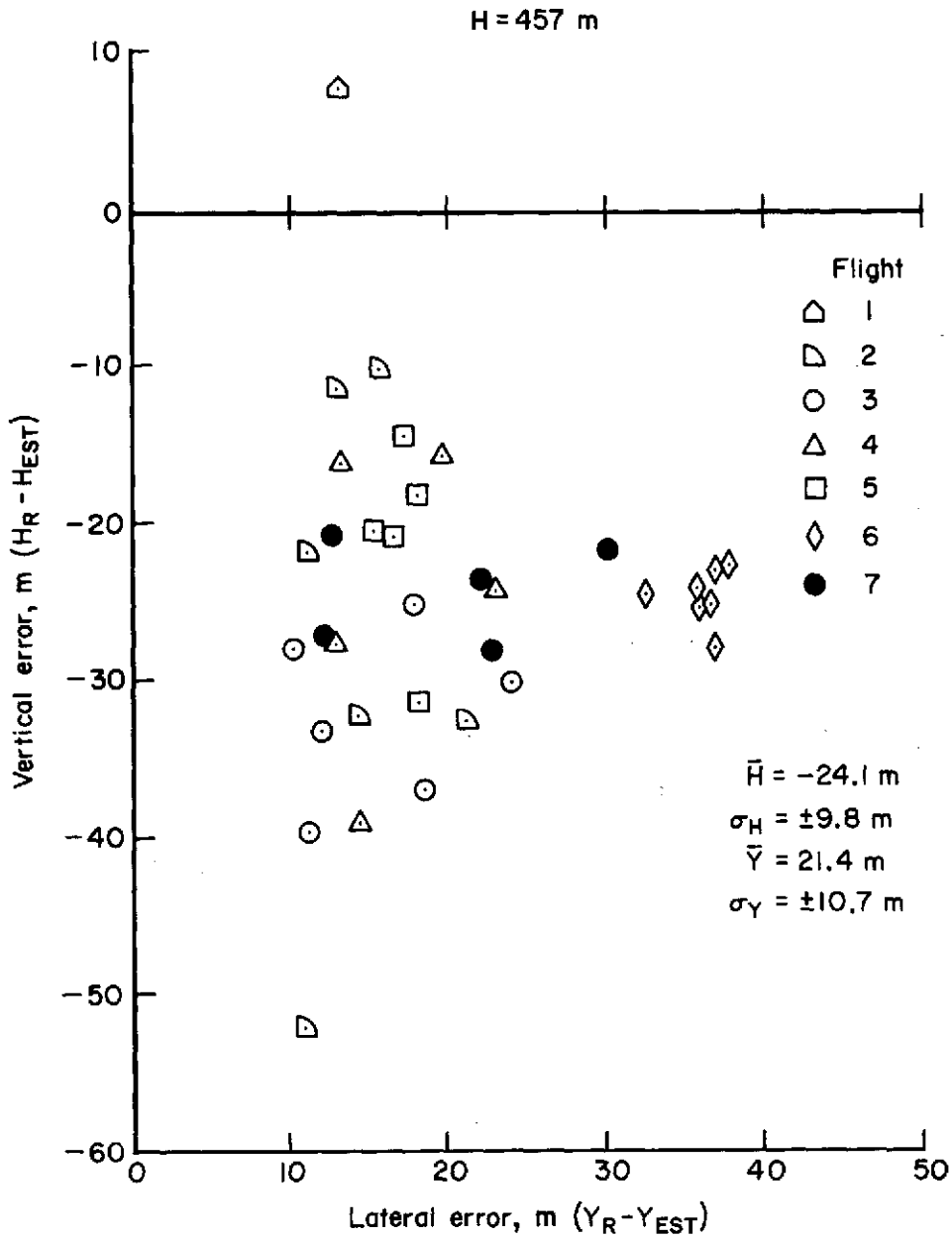

Figure 29.– Navigation errors at first flare window.

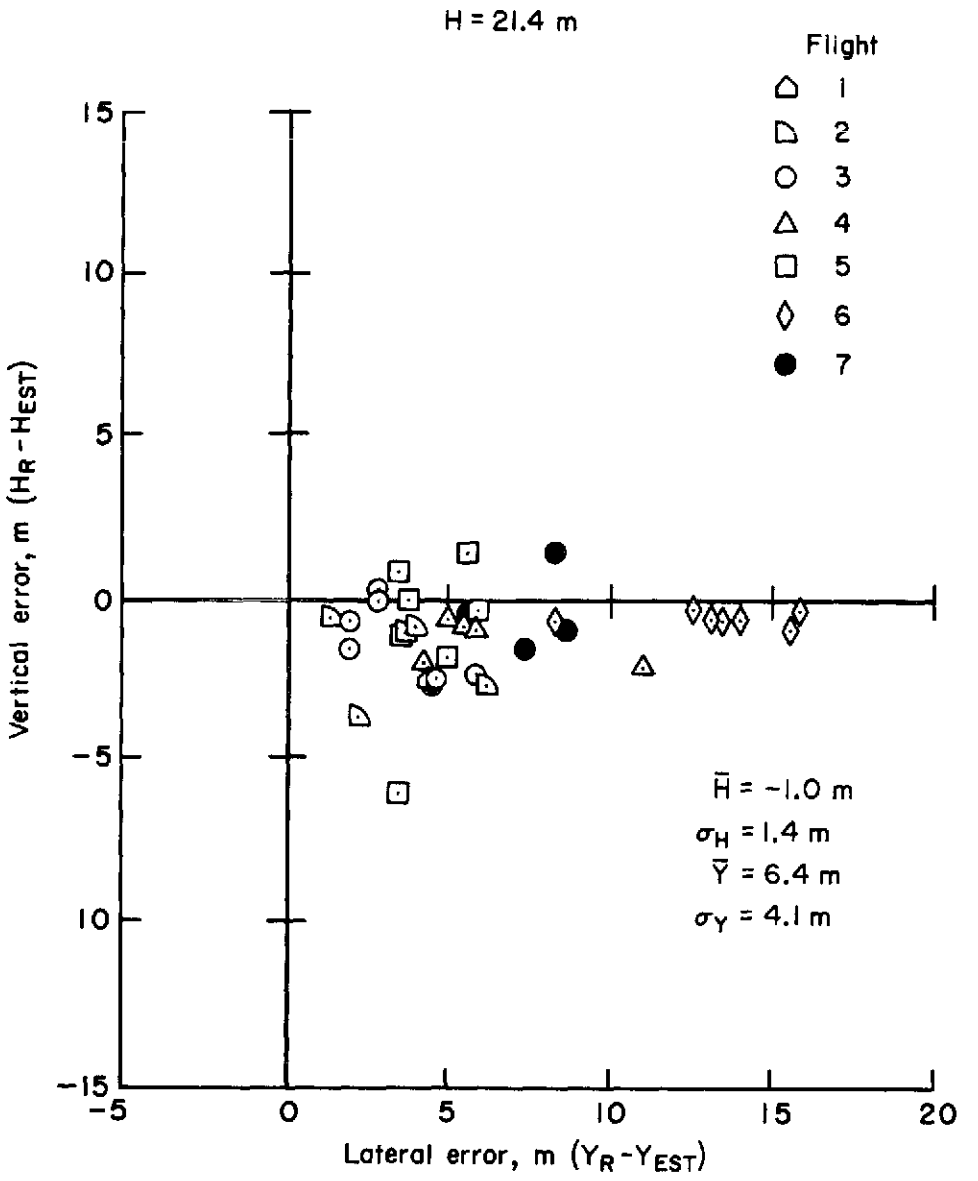

Figure 30.– Navigation errors at final flare window.

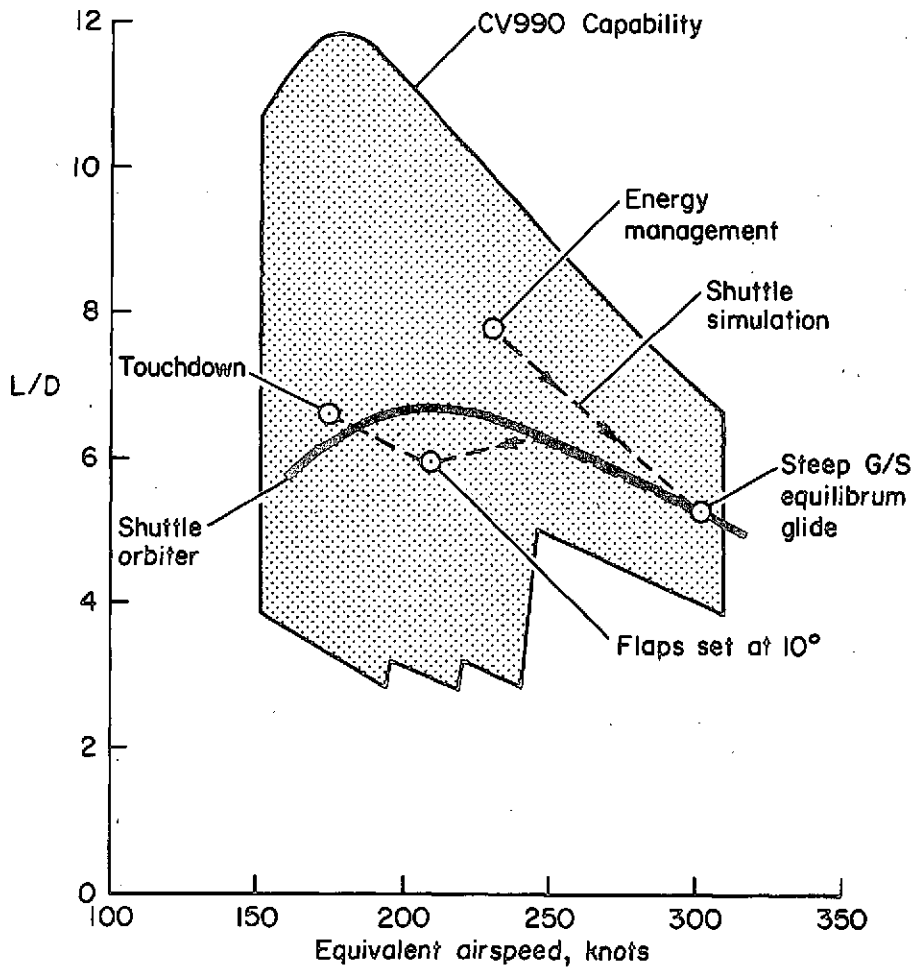

Figure 31.– Lift/drag ratio comparison of CV-990 shuttle simulation with typical delta wing shuttle orbiter (unpowered).